

Pulse-area theorem in a single-mode waveguide and its application to photon echo and optical memory in $\text{Tm}^{3+}:\text{Y}_3\text{Al}_5\text{O}_{12}$

S. A. Moiseev^{1,*}, M. M. Minnegaliev¹, E. S. Moiseev¹, K. I. Gerasimov¹, A. V. Pavlov¹,
T. A. Rupasov¹, N. N. Skryabin², A. A. Kalinkin² and S. P. Kulik^{2,3}

¹Kazan Quantum Center, Kazan National Research Technical University n.a. A.N. Tupolev-KAI, 10 K. Marx St., 420111, Kazan, Russia

²Quantum Technologies Center and Faculty of Physics, M.V. Lomonosov Moscow State University, Leninskie Gory, 119991, Moscow, Russia

³Laboratory of Quantum Engineering of Light, South Ural State University (SUSU), Lenin Avenue, 454080, Chelyabinsk, Russia



(Received 24 October 2022; accepted 27 March 2023; published 20 April 2023)

We derive the area theorem for light pulses interacting with an inhomogeneously broadened ensemble of two-level atoms in a single-mode optical waveguide and present its analytical solution for Gaussian-type modes, which demonstrates the significant difference from the formation of 2π pulses by plane waves. We generalize this theorem to the description of photon echo and apply it to the two-pulse (primary) echo and the revival of silenced echo (ROSE) protocol of photon echo quantum memory. We implemented ROSE protocol in a single-mode laser-written waveguide made of an optically thin crystal $\text{Tm}^{3+}:\text{Y}_3\text{Al}_5\text{O}_{12}$. The experimental data obtained are satisfactorily explained by the developed theory. Finally, we discuss the obtained experimental results and possible applications of the derived pulse-area approach.

DOI: [10.1103/PhysRevA.107.043708](https://doi.org/10.1103/PhysRevA.107.043708)

I. INTRODUCTION

The coherent interaction of a light pulse with resonant atomic ensembles plays a significant role in modern optics and quantum technologies [1–4]. These interactions often pose nonlinear character, study of which is a difficult theoretical task. The pulse-area theorem [5] provides a simple but powerful tool for general analysis of nonlinear coherent light-atoms dynamics in self-induced transparency [5], optical solitons [6], superradiance [7], photon echo in optically dense media [8–10], to name a few. The approach was developed for propagating plane light waves that interact with atoms in free space. Recent progress in integrated quantum photonics [11–14] motivates the study of the coherent interaction between light pulses and resonant atomic ensembles in optical waveguides, where the development of waveguide optical quantum memory (QM) attracts growing attention [15–20].

The goal of an optical QM is to store quantum states of light for subsequent on-demand retrieval at an arbitrary time [21–26]. QM is a vital component for numerous quantum technologies, such as long-distance quantum communications [4,27,28], quantum state preparation [29], and a synchronization unit for optical quantum processing [24].

Great promises are associated with the photon-echo-based optical QM in crystals doped with *rare-earth ions* (REI) [23] that have a long lifetime of quantum coherence at optical and microwave transitions. Such optical QM has advantages in its multiplexing capacity for storing a large number of temporary light modes and demonstrates high efficiency in REI-doped crystals, for example, 58% in the cavity assistant scheme [30] and 69% in the free space [31], which are comparable to

the 76% efficiency of single-mode storage achieved with QM protocol based on electromagnetically induced transparency in REI-doped crystal [32].

Currently, there is growing interest in the implementation of photon echo QM in optical waveguides [16,18,33–35] doped by REIs which seem as a convenient platform for implementation of on-chip QM. Quantum storage in REI-doped waveguides was demonstrated in experiments on heralded single-photon storage [36,37], on-demand qubit storage [19], and frequency-multiplexed storage [38]. All of the above experiments are based on the scheme of reversible photon echo in an optically dense medium [39–41], realized for inhomogeneous broadening in the form of a periodic narrow *atomic frequency combs* that is called AFC protocol [42]. There is a particular interest in the *revival of silenced echo* (ROSE) protocol [43,44] for implementation of optically controlled on-demand QM with low quantum noise background in atomic ensemble with naturally inhomogeneous broadening and narrow homogeneous lines that is embedded in an optical waveguide.

Recently the ROSE protocol was implemented in the $^{151}\text{Eu}^{3+}:\text{Y}_2\text{SiO}_5$ crystal with the type-II single-mode laser-written waveguide [35]. This type of the waveguide supports propagation of light modes with only one polarization. At the same time, light modes of arbitrary polarization can propagate in a type-III waveguide. Such type-III depressed cladding single-mode waveguides were fabricated by femtosecond laser writing technique in the crystal $\text{Tm}^{3+}:\text{Y}_3\text{Al}_5\text{O}_{12}$ [45]. Therefore, it is desirable to implement the ROSE protocol in this waveguide, which is the subject of experimental studies of this work.

The mentioned need for a highly efficient implementation of photon echo QMs and its integration with waveguide schemes makes it relevant to develop a general theoretical

*s.a.moiseev@kazanqc.org

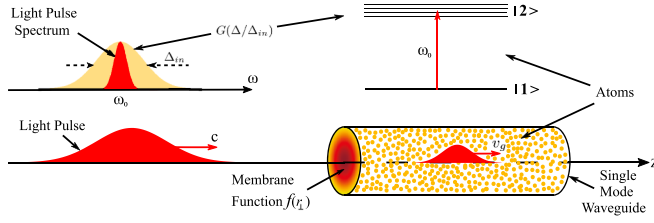


FIG. 1. Spatial scheme of interaction of light pulses with an ensemble of two-level atoms in a single-mode optical waveguide. $G(\Delta/\Delta_{in})$ is an inhomogeneous broadening with linewidth Δ_{in} , c and v_g are the speeds of light in free space and in the waveguide; $f(\mathbf{r}_\perp)$ is a membrane function of light field in the the single-mode waveguide.

approach for describing the coherent interaction between light and atoms in optical waveguides. The approach should properly simulate the application of intense control laser fields, e.g., π pulses, that induce nonlinear dynamics in resonant atoms.

Since the McCall-Hahn work [5], it was discovered that the most general patterns of linear and nonlinear interaction between light pulses and coherent two-level media can be described by the area theorem [1,6,7]. The area theorem was also applied to the description of photon echo in optically dense media [8,9,46,47], in Fabry-Perot resonator [10], as well as it was applied for studies of photon echo CRIB protocol in free space [48] and for description of cavity assistant ROSE protocol [44]. It is worth noting that in recent experiments [44,47], it has been found that in media with a symmetrical form of inhomogeneous broadening, the behavior of the pulse area of the echo signal almost flatly reproduces the behavior of the amplitude of echo signals. It makes this approach universal for describing linear and nonlinear behavior in various scenarios of photon echo, as well as photon-echo-based QM protocols in optically dense resonant media.

In this work, we derive the *waveguide pulse area* (WPA) theorem for the resonant interaction between light pulse and two-level atoms in a single-mode optical waveguide (see Fig. 1). We found the analytical form of the WPA theorem, demonstrating significant differences in a formation of stable 2π pulses compared to the well-known McCall-Hahn pulse area theorem [5]. Then we generalize WPA theorem for the echo signal emission and apply it for description of the two-pulse (primary) photon echo and ROSE protocol of photon echo QM. We present experimental results on ROSE protocol in a laser-written waveguide of a Tm^{3+} crystal: $\text{Y}_3\text{Al}_5\text{O}_{12}$. Then we discuss the obtained experimental data using the WPA theorem, focusing on the factors leading to a negative impact on the efficiency of the QM protocol implementation and outlining the possible applications of the developed theoretical approach to other problems.

II. WAVEGUIDE PULSE-AREA THEOREM

A. Maxwell-Bloch equations in single-mode waveguide and pulse-area theorem

We derive the equations of motion by starting with the Hamiltonian \hat{H}_0 , which is composed of Hamiltonian of

noninteracting two-level atoms \hat{H}_a with inhomogeneously broadened resonant transition, Hamiltonian of waveguide light modes \hat{H}_f , and an interaction Hamiltonian between the atoms and waveguide modes in dipole and rotating-wave approximations \hat{V}_{fa} :

$$\hat{H}_0 = \hat{H}_a + \hat{H}_f + \hat{V}_{fa}. \quad (1)$$

We consider the free atomic Hamiltonian to contain several types of two-level atoms with different dipole moments of resonant transition \mathbf{d}_m . It is a typical case with rare-earth ions, where active ions may substitute for host atoms at different positions in a crystal, leading to several (M) groups of atoms with different dipole moments [49]. The free atomic Hamiltonian is

$$\hat{H}_a = \sum_{m=1}^M \sum_{j=1}^{N_m} \frac{\hbar}{2} (\omega_0 + \Delta_j) \sigma_{3,m}^j, \quad (2)$$

where N_m is a number of atoms within m th group, ω_0 is the carrier frequency of the light field coinciding with the center of the line of the optical atomic transition (see Fig. 1), $\sigma_{1,m}^j, \sigma_{2,m}^j, \sigma_{3,m}^j$ are standard set of Pauli matrices related to the j th two-level atom from m th group, Δ_j is detuning of j th atom from the carrier frequency.

The Hamiltonian of the waveguide light mode propagating along the z direction is [50–52]

$$\hat{H}_f = \hbar \int dz a^\dagger(z) \left[\omega_0 a(z) - iv_g \frac{\partial}{\partial z} a(z) \right], \quad (3)$$

where $v_g = \frac{\partial \omega_0}{\partial \beta}$ is a group velocity (see Fig. 1), $\beta = \sqrt{k^2(\omega_0) - (2\pi/\Lambda)^2}$, $k(\omega) = n(\omega)\omega/c$, $n(\omega) = \sqrt{\varepsilon(\omega)}$, $\varepsilon(\omega)$ is an electric permittivity of dielectric medium and Λ being a critical waveguide wavelength [53], $a(z)$ [$a^\dagger(z)$] is bosonic annihilation (creation) operator of light field mode at given coordinate z with commutation relation $[\hat{a}(z), \hat{a}^\dagger(z')] = \delta(z - z')$. The operators are expressed with a help of their one-dimensional Fourier image $a(k)$:

$$\hat{a}(z) = \frac{1}{\sqrt{2\pi}} \int dk e^{i(k-\beta)z} a(k). \quad (4)$$

The electric field of the waveguide mode [54], taking into account their structure in an optical waveguide, has the form

$$\hat{\mathbf{E}}(\mathbf{r}) = i\mathbf{e}E_0 f(\mathbf{r}_\perp) \hat{a}(z) e^{i\beta z} + \text{H.c.}, \quad (5)$$

where $E_0 f(\mathbf{r}_\perp)$ is a single-photon electric field amplitude [2] at the point \mathbf{r}_\perp in the transverse plane of the single-mode waveguide with reference frame being chosen as $\mathbf{r}^j = \mathbf{r}_\perp^j + z_j \mathbf{e}_z$. $f(\mathbf{r}_\perp)$ is a membrane function of the light mode [53,55], \mathbf{e} is a polarization vector of the light field, $E_0 \cong (\frac{\hbar\omega_0}{2\varepsilon_0\varepsilon(\omega_0)S})^{1/2}$, \hbar is reduced Planck's constant, S is the cross section of the light beam, and ε_0 is the electric permittivity of vacuum, respectively [2]. We assume that permittivity of the dielectric medium is constant and does not change over the bandwidth of interest.

The interaction Hamiltonian between the atoms and the waveguide mode in the rotating-wave approximation takes the

form

$$\hat{V}_{fa} = -\frac{\hbar}{2} \sum_{m=1}^M \sum_{j=1}^{N_m} \Omega_{0,m}(\mathbf{r}_\perp^j) \sigma_{-,m}^j \hat{a}^\dagger(z_j) e^{-i\beta z_j} + \text{H.c.}, \quad (6)$$

where $\sigma_{\pm,m}^j = \frac{1}{2}(\sigma_{1,m}^j \pm i\sigma_{2,m}^j)$ are the isospin flip operators for j th atom of m th group, $\Omega_{0,m}(\mathbf{r}_\perp^j) = \Omega_m f(\mathbf{r}_\perp^j)$ is a coupling constant between j th atom of m th group and waveguide mode with $\Omega_m = E_0(\mathbf{d}_m \cdot \mathbf{e})/\hbar$ being a single-photon Rabi frequency of j th atom located at \mathbf{r}^j . The membrane function $f(\mathbf{r}_\perp)$ determines the dependence of the interaction constant of an atom on its position \mathbf{r}_\perp in the transverse plane of the waveguide. For sake of simplicity but without losing generality, we assume $f(\mathbf{r}_\perp)$ to be a real-valued function.

We introduce slowly varied operators

$$\hat{a}_p(z, t) = i e^{i\omega_0 t - i\beta z} \hat{a}(z, t), \quad (7)$$

$$\hat{\sigma}_{-,m}^j(t) = e^{i\omega_0 t - i\beta z} \hat{\sigma}_{-,m}^j, \quad (8)$$

$$\hat{\sigma}_{+,m}^j(t) = e^{-i\omega_0 t + i\beta z} \hat{\sigma}_{+,m}^j, \quad (9)$$

with the same commutation relations as $\hat{a}(z, t)$, $\hat{\sigma}_{-,m}^j(t)$, and $\hat{\sigma}_{+,m}^j(t)$, respectively. The index p in $a_p(z, t)$ indicates name of the studied pulse for further echo analysis, i.e., $p = (s, 1, 2, e)$ correspond to signal, first control, second control, and echo pulses, respectively.

The resulted Heisenberg equations for the slowly varied operators are

$$\left(\frac{\partial}{\partial t} + v_g \frac{\partial}{\partial z} \right) \hat{a}_p(z, t) = \frac{i}{2} \sum_{m=1}^M \sum_{j=1}^{N_m} \Omega_{0,m}(\mathbf{r}_\perp^j) \hat{\sigma}_{-,m}^j(t) \delta(z - z_j), \quad (10)$$

$$\frac{\partial \hat{\sigma}_{-,m}^j}{\partial t} = -i\Delta_j \hat{\sigma}_{-,m}^j - \frac{i}{2} \Omega_{0,m}(\mathbf{r}_\perp^j) \hat{a}_p(z_j, t) \sigma_{3,m}^j, \quad (11)$$

$$\frac{\partial \hat{\sigma}_{+,m}^j}{\partial t} = i\Delta_j \hat{\sigma}_{+,m}^j + \frac{i}{2} \Omega_{0,m}(\mathbf{r}_\perp^j) \hat{a}_p^\dagger(z_j, t) \sigma_{3,m}^j, \quad (12)$$

$$\frac{\partial \sigma_{3,m}^j}{\partial t} = -i\Omega_{0,m}(\mathbf{r}_\perp^j) [\hat{a}_p^\dagger(z_j, t) \hat{\sigma}_{-,m}^j - \hat{a}_p(z_j, t) \hat{\sigma}_{+,m}^j]. \quad (13)$$

It is worth noting that at relatively large number of atoms with negligible small change of the population $[\sigma_{3,m}^j(t) \cong \sigma_{3,m}^j(t_0)]$, the system of Eqs. (10)–(13) is linearized. Such conditions are often used in different photon echo quantum memory schemes [23,56,57], where their solutions can be found for the arbitrary quantum states of lights.

The operators in Eqs. (10)–(13) can be simplified in classical limit of light field into c -number equations on average values of the operators by a proper splitting of two-particle correlators. For an atomic ensemble with large N_m and the waveguide mode being in coherent state we replace the product of operator by a product of their mutual average values [1,58]

$$\langle \hat{a}_p^{(\dagger)}(z_j, t) \sigma_{3,m}^j(t) \rangle \cong \langle \hat{a}_p^{(\dagger)}(z_j, t) \rangle \langle \sigma_{3,m}^j(t) \rangle, \quad (14)$$

$$\langle \hat{a}_p^{(\dagger)}(z_j, t) \sigma_{+(-),m}^j(t) \rangle \cong \langle \hat{a}_p^{(\dagger)}(z_j, t) \rangle \langle \sigma_{+(-),m}^j(t) \rangle. \quad (15)$$

For further convenience we switch to real-value equations by separating the constant phase shift ϕ_0 and amplitude from the averaged field operator $\langle \hat{a}_0(z, t) \rangle = a_0(z, t) e^{i\phi_0}$ and including the phase shift in the atomic operators $\sigma_{\pm,m}^j(t) = e^{-i\phi_0} \sigma_{0,\pm,m}^j(t)$, $\sigma_{-,m}^j(t) = e^{i\phi_0} \sigma_{0,-,m}^j(t)$. Finally, by switching to the components of Bloch vector for j_m atom

$$v_m^j(t) = i[\langle \sigma_{0,-,m}^j(t) \rangle - \langle \sigma_{0,+,m}^j(t) \rangle], \quad (16)$$

$$u_m^j(t) = \langle [\sigma_{0,-,m}^j(t) + \sigma_{0,+,m}^j(t)] \rangle, \quad (17)$$

$$w_m^j(t) = \langle \sigma_{3,m}^j(t) \rangle, \quad (18)$$

we get the following system of equations:

$$\begin{aligned} & \left(\frac{\partial}{\partial t} + \frac{\gamma_w}{2} + v_g \frac{\partial}{\partial z} \right) a_p(z, t) \\ & = \sum_{m=1}^M \sum_{j=1}^{N_m} \frac{\Omega_{0,m}(\mathbf{r}_\perp^j)}{4} v_m^j(t) \delta(z - z_j), \end{aligned} \quad (19)$$

$$\frac{\partial u_m^j(t)}{\partial t} = -\frac{\gamma}{2} u_m^j(t) - \Delta_j v_m^j(t), \quad (20)$$

$$\begin{aligned} \frac{\partial v_m^j(t)}{\partial t} & = -\frac{\gamma}{2} v_m^j(t) + \Delta_j u_m^j(t) \\ & + \Omega_{0,m}(\mathbf{r}_\perp^j) a_p(z_j, t) w_m^j(t), \end{aligned} \quad (21)$$

$$\frac{\partial w_m^j(t)}{\partial t} = -\Omega_{0,m}(\mathbf{r}_\perp^j) a_p(z_j, t) v_m^j, \quad (22)$$

where we have added phenomenologically the decay constant γ_w describing nonresonant losses of the waveguide modes and the decay constant of atomic phase relaxation $\gamma = 2/T_2$ (see Appendix A, where the decay constants γ_w and γ are introduced together with the related Langevin forces). Although Eqs. (19)–(22) do not describe all the quantum properties of light and atoms, they are sufficient for analyzing the efficiency, coherence, and spectral properties of optical QM for weak light fields.

Next, we derive a pulse-area theorem for general description of the nonlinear properties of coherent interaction of light pulse with two-level medium in a single-mode optical waveguide. The presence of several dipole moments makes it difficult to define the total pulse area of the atomic ensemble. Hence, instead of pulse area, we define *envelope area* of the field that is agnostic to the presence of several dipole moments

$$\theta_p(z) = \int_{t_0}^{t_0 + \delta t_f} dt a_p(z, t). \quad (23)$$

We assume that pulse duration of the light pulses δt_f is significantly shorter than the phase relaxation time of the atomic transition ($\gamma \delta t_f \ll 1$). By integrating Eq. (19) over a duration of the light pulse from its beginning t_0 to its end similarly to [1,5] and using formal solution $r_m^j(t) = v_m^j(t) + iu_m^j(t)$ of Eqs. (20)–(22) with initial condition $v_m^j(t_0) = 0$, $w_m^j(t_0) =$

w_0 , we get the equation for the envelope area

$$\begin{aligned} \left(\frac{\partial}{\partial z} + \frac{\gamma_w}{2v_g}\right)\theta_p(z) &= \text{Re} \left\{ \sum_{m=1}^M \sum_{j=1}^{N_m} \frac{\Omega_{0,m}(\mathbf{r}_\perp^j)}{4v_g} \int_{t_0}^{t \gg \delta t_f} dt r_m^j(t) \right\} \delta(z - z_j) \\ &= \text{Re} \left\{ \sum_{m=1}^M \sum_{j=1}^{N_m} \frac{\Omega_{0,m}^2(\mathbf{r}_\perp^j)}{4v_g} \int_{t_0}^{t \gg \delta t_f} dt \int_{t_0}^t dt' e^{-(\gamma/2 + i\Delta_j)(t-t')} a_p(z_j, t') w_m^j(t') \right\} \delta(z - z_j). \end{aligned} \quad (24)$$

Taking into account that $a_p(z_j, t \gg \delta t_f) = 0$, we can extend the limits of integration over time from $\int_{t_0}^{t \gg \delta t_f} dt \dots$ to $\int_{t_0}^{\infty} dt \dots$. By changing the order of integration further $\int_{t_0}^{\infty} dt \int_{t_0}^t dt' \dots \rightarrow \int_{t_0}^{\infty} dt' \int_{t_0}^{\infty} dt \dots$ and performing integration over t we find

$$\begin{aligned} \left(\frac{\partial}{\partial z} + \frac{\gamma_w}{2v_g}\right)\theta_p(z) &= \text{Re} \left\{ \sum_{m=1}^M \sum_{j=1}^{N_m} \frac{\Omega_{0,m}^2(\mathbf{r}_\perp^j)}{4v_g} \frac{1}{\gamma/2 + i\Delta_j} \int_{t_0}^{\infty} dt' a_p(z_j, t') w_m^j(t') \right\} \delta(z - z_j) \\ &= \sum_{m=1}^M \sum_{j=1}^{N_m} \frac{\frac{1}{2}\gamma \Omega_{0,m}^2(\mathbf{r}_\perp^j)}{4v_g(\frac{1}{4}\gamma^2 + \Delta_j^2)} \int_{t_0}^{\infty} dt' \alpha_p(z_m^j, t') w_m^j(t') \delta(z - z_j). \end{aligned} \quad (25)$$

The coupling constant between an atom and light mode $\Omega_{0,m}(\mathbf{r}_\perp)$ is contained in the equations for the components of the Bloch vector (19), (21), (22) and in the equation for the envelope area (25). For further convenience the summation of an arbitrary function $F_m(\mathbf{r}_\perp^j, z_j, \Delta_j, t)$ over the atoms in continuous limit may be approximated as an integration

$$\sum_{j=1}^{N_m} F_m(\mathbf{r}_\perp^j, z_j, \Delta_j, t) \delta(z - z_j) = \rho_m \int d\Delta G\left(\frac{\Delta}{\Delta_{in}}\right) \int_S dx dy F_m(\mathbf{r}_\perp, z, \Delta, t), \quad (26)$$

where S is a cross section of the waveguide, $\rho_m = \frac{N_m}{LS}$ is a density of m th atomic group with L being length the waveguide. For sake of simplicity we assume the identical inhomogeneous broadening profiles $G(\frac{\Delta}{\Delta_{in}})$ for different atomic groups with linewidth Δ_{in} . Substituting Eq. (26) in (25) we get

$$\left(\frac{\partial}{\partial z} + \frac{\gamma_w}{2v_g}\right)\theta_p(z) = \sum_{m=1}^M \frac{\pi \rho_m}{4v_g} \int_S dx dy \Omega_{0,m}(\mathbf{r}_\perp) \int d\Delta \frac{\frac{1}{2}\gamma G(\frac{\Delta}{\Delta_{in}})}{\pi(\frac{1}{4}\gamma^2 + \Delta^2)} \Omega_{0,m}(\mathbf{r}_\perp) \int_{t_0}^{\infty} dt' \alpha_p(z, t') w_m(\mathbf{r}_\perp, z, \Delta, t'). \quad (27)$$

For large enough inhomogeneous broadening ($\Delta_{in} \gg \gamma$) single-atom spectral response is assumed to be delta function $\frac{\gamma}{\pi(\gamma^2 + \Delta^2)} \cong \delta(\Delta)$. If there is not any initial coherence $v_m^j(t_0) = 0$, the solution for resonant atomic coherence in Eqs. (21) and (22) is

$$\Omega_{0,m}(\mathbf{r}_\perp) \int_{t_0}^{t \gg \delta t_f} dt' \alpha_p(z_m^j, t') w_m(\mathbf{r}_\perp, z, \Delta = 0, t') = v_m(\mathbf{r}_\perp, z, \Delta = 0, t)|_{t_0}^t = w_m^j(t_0) \sin[\Theta_{m,p}(\mathbf{r}_\perp, z)], \quad (28)$$

where $\Theta_{m,p}(\mathbf{r}_\perp, z) = \Omega_{0,m}(\mathbf{r}_\perp) \theta_p(z)$ is a conventional pulse area of m th atom located at a point with coordinates (\mathbf{r}_\perp, z) . Substituting the initial condition for population $w_m^j(t_0) = -1$ and using $\delta(\Delta)$ in Eq. (27), we get the following equation for the envelope area $\theta_p(z)$:

$$\left(\frac{\partial}{\partial z} + \frac{\gamma_w}{2v_g}\right)\theta_p(z) = -\Phi(\theta_p), \quad (29)$$

where

$$\Phi(\theta_p) = \sum_{m=1}^M \frac{\xi_m}{2} \int_S dx dy \Omega_{0,m}(\mathbf{r}_\perp) \sin[\Theta_{m,p}(\mathbf{r}_\perp, z)]. \quad (30)$$

The atomic function $\Phi(\theta_p)$ describes the contribution of the total polarization within the fiber cross section $\xi_m = \frac{\pi G(0)\rho_m}{2v_g}$, where for large Δ_{in} we can use $G(\frac{\Delta}{\Delta_{in}}) = \frac{\Delta_{in}}{\pi(\Delta_{in}^2 + \Delta^2)}$. Equation (29) represents waveguide pulse-area (WPA) theorem, which is an analog of the pulse-area theorem for two-level atoms interacting in general waveguide mode. Below, we dis-

cuss several examples of the application of WPA theorem to Gaussian and Gaussian-type profiles of the waveguide modes.

B. Gaussian mode

The solution of Eq. (29) strongly depends on the transverse properties of the waveguide modes. In the simplest case of a plane wave, where the field amplitude is spatially homogeneous in the cross section [$f(\mathbf{r}_\perp) = f_h(\mathbf{r}_\perp) = 1$], we get an atomic function containing just the sum of the known terms corresponding to various dipole moments (see also [59]):

$$\Phi(\theta_p) = \sum_{m=1}^M \frac{S \xi_m \Omega_m}{2} \sin(\Omega_m \theta_p). \quad (31)$$

For $M = 1$ the derived Eq. (30) is reduced to the well-known McCall-Hahn pulse-area theorem for the light pulse propagation in free space [1,5]. In the limit of large optical depth the pulse area of the input pulse tends to $\Theta(\infty) \gg 1 \rightarrow 2n\pi$ for the initial pulse area of $(2n - 1)\pi < \Theta(0) < (2n +$

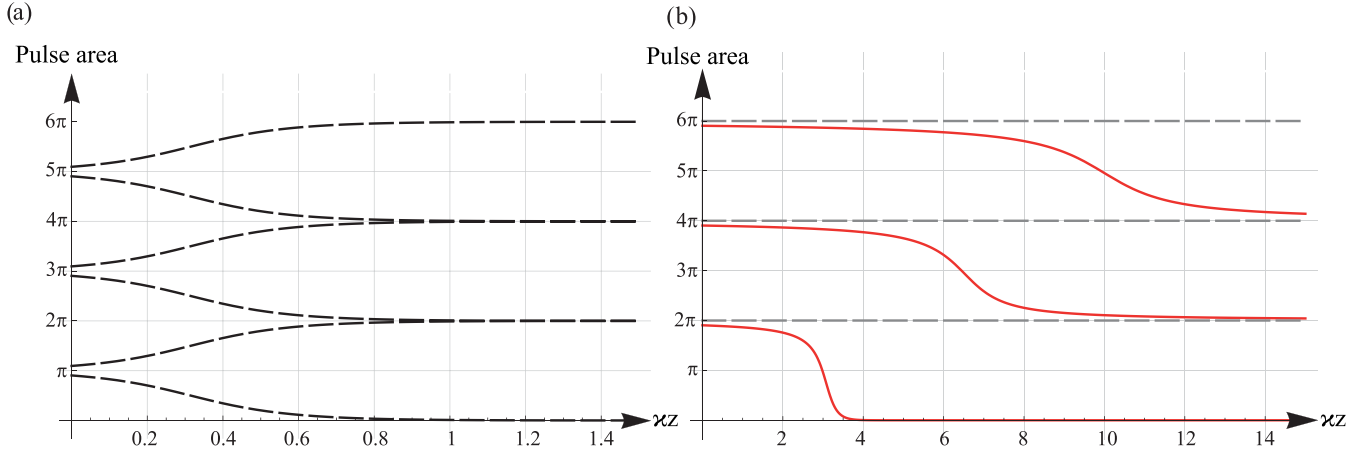


FIG. 2. (a) Pulse area $\Theta_p(z)$ of McCall-Hahn area theorem [5] versus optical depth κz for different input pulse areas [$\Theta_p(0) : \pi \pm 0.1, 3\pi \pm 0.1, 5\pi \pm 0.1$]; (b) pulse area $\Theta_p(z)$ of WPA theorem (39) versus optical depth κz for different input pulse areas [$\Theta_p(0) : 2\pi - 0.2, 4\pi - 0.2, 6\pi - 0.2$]; the optical densities of atomic ensembles in the waveguide and in free space are assumed to be equal.

$1)\pi$ as it is shown in Fig. 2(a). Here, $\kappa_m = \pi a^2 \Omega_m^2 \xi_m = \frac{\rho_m \omega}{4v_g \epsilon_0 \epsilon \hbar} |\langle \mathbf{d}_m \cdot \mathbf{e} \rangle|^2$ is a resonant absorption coefficient of m th atomic group and $S = \pi a^2$ with a being a radius of the waveguide.

For the transverse light mode with a Gaussian membrane function

$$f(\mathbf{r}_\perp) = f_g(\mathbf{r}_\perp) = \exp\left\{-\frac{(x^2 + y^2)}{2a^2}\right\} \quad (32)$$

the integration over the cross section in Eq. (30) gives the following equation on the envelope area:

$$\left(\frac{\partial}{\partial z} + \frac{\gamma_w}{2v_g}\right)\theta_p = -\sum_{m=1}^M \frac{\kappa_m \sin^2(\Omega_m \theta_p/2)}{\Omega_m \theta_p/2}. \quad (33)$$

For Gaussian mode WPA theorem shows that $\frac{\partial}{\partial z}\theta_p(z) < 0$ for $2n\pi < \Theta_{m,p} < 2(n+1)\pi$ with $n \in \{0, 1, 2, \dots\}$ and $\Theta_{m,p} = \Omega_m \theta_p$ being conventional pulse area of the m th resonant atoms without spatial dependence as if the m th atoms were located in the center of the waveguide. At the same time, $\frac{\partial}{\partial z}\theta_p(z) = 0$ for $\Theta_{m,p} = 2n\pi$ and negligibly weak nonresonant losses ($\frac{\gamma_w L}{2v_g} \ll 1$). In other words, if the initial pulse area $\Theta_{m,p}(0)$ is less than 2π , at the output the pulse area decreases to zero. This fact distinguishes the WPA theorem from the McCall-Hahn theorem [5], where 2π pulse is formed even if $\Theta_{m,p}(0) > \pi$.

Similarly as in the plane-wave case, in the limit of small pulse area Eq. (33) is reduced to the linearized Lambert-Beer equation

$$\frac{\partial}{\partial z}\theta_s(z) = -\frac{1}{2}\left(\frac{\gamma_w}{v_g} + \sum_{m=1}^M \kappa_m\right)\theta_s(z), \quad (34)$$

with exponential solution

$$\theta_s(z) = \theta_s(0)e^{-\alpha z/2}, \quad (35)$$

where $\alpha = \frac{\gamma_w}{v_g} + \sum_{m=1}^M \kappa_m$ is a total absorption coefficient. In the case of only a single atomic type, i.e., $M = 1$ and

$\Theta_{m,p}(z) = \Theta_p(z)$, Eq. (33) is simplified to

$$\left(\frac{\partial}{\partial z} + \frac{\gamma_w}{2v_g}\right)\Theta_p = -\kappa_1 \frac{\sin^2(\Theta_p/2)}{\Theta_p/2}. \quad (36)$$

C. Gaussian-type modes

The other remarkable example is application of WPA theorem to the interaction of light pulse with two-level atoms in a typical single-mode optical fiber. The membrane function of a quasilinearly polarized mode in the single-mode fiber is often described by a zero-order Bessel function [55]. Here, we consider two possible cases for filling the fiber with two-level atoms. In the first case [$f_1(\mathbf{r}_\perp)$], the atoms are evenly distributed inside the fiber core, and in the second case [$f_2(\mathbf{r}_\perp)$], they are also located in the fiber cladding, filling the entire fiber volume evenly. The membrane functions of light modes in these two cases are

$$f_1(\mathbf{r}_\perp) = \begin{cases} J_0(ur_\perp/a), & r_\perp \leq a \\ 0, & r_\perp > a \end{cases} \quad (37)$$

$$f_2(\mathbf{r}_\perp) = \begin{cases} J_0(ur_\perp/a), & r_\perp \leq a \\ \frac{J_0(u)}{K_0(w)} K_0(wr_\perp/a), & r_\perp > a \end{cases} \quad (38)$$

where $J_0(x)$ is Bessel function of the first kind, $K_0(x)$ is modified Bessel function of the second kind, u is the normalized transverse phase constant, w is normalized transverse attenuation constant (propagation constant), and a is a fiber core radius.

We compare properties of these Gaussian-type modes to the derived Gaussian mode assuming presence of uniformly distributed single atomic species. We numerically integrate the right-hand side of Eq. (30) for $f_{1,2}(\mathbf{r}_\perp)$ and $f_g(\mathbf{r}_\perp)$. The resulted functions $\frac{\Omega_1}{\kappa_1} \Phi_{g,1,2}(\theta_p)$ describe the contributions of the total polarization in the equation for given envelope area as it is in Fig. 3. The Gaussian and Bessel modes give very similar results for their atomic functions $\Phi_g(\theta_p)$ and $\Phi_2(\theta_p)$, which are greater than zero for any z . A significantly noticeable difference between these two functions occurs only starting from the second minimum at $\Theta = 4\pi$, where the

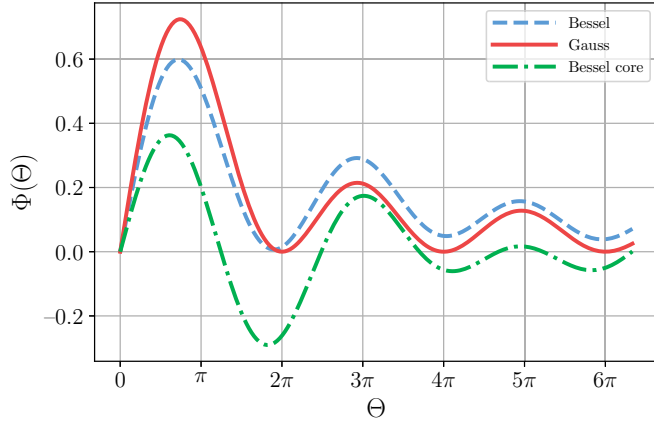


FIG. 3. The atomic functions $\Phi_{g,1,2}(\Theta)$ for Gaussian, Bessel, and Bessel core membrane functions $f_{g,1,2}(\mathbf{r}_\perp)$.

function $\Phi_2(\theta_p)$ becomes nonzero. When atoms are uniformly distributed only inside the fiber core, the function $\Phi_1(\theta_p)$ has the form of a damped oscillatory function. Similarly to the McCall-Hahn area theorem, the branching points of the solution also appear at $\Theta_p \approx 1.25\pi$, $\Theta_p \approx 3.75\pi, \dots$, where the solution of pulse area $\Theta_p(z)$ increases from the branching points to the values of 2.5π and 4.5π . The similar quantitative and qualitative behaviors of $\Phi_g(\theta_p)$ and $\Phi_2(\theta_p)$ allow to use the analytical solution of the Gaussian mode for description of the both cases at $\Theta_p(0) < 4\pi$.

D. Evolution in optically dense medium

We study the evolution of the pulse area in a waveguide with Gaussian mode and optically dense medium. For a single atomic group and negligibly weak nonresonant absorption $\frac{\gamma_w z}{2v_g} \ll 1$, the exact analytical solution of Eq. (36) is

$$T_n(\Theta_p(z)) = T_n(\Theta_p(0)) - \frac{\varkappa_1}{2} z, \quad (39)$$

where $T_n(\Theta_p)$ is given by

$$T_n(\Theta_p) = \ln \left[\sin \left(\frac{\Theta_p}{2} \right) \right] - \frac{\Theta_p}{2} \cot \frac{\Theta_p}{2}. \quad (40)$$

Analytical solution of Eqs. (39) and (40) clearly reveals distinctive features of pulse-area evolution in the optically dense single-mode optical waveguides. Figures 2(a) and 2(b) show the behavior of the pulse areas for the McCall-Hahn area theorem and for the WPA theorem, respectively. According to McCall-Hahn theorem [5], 2π pulse are generated for initial pulse area $\pi < \Theta_p(0) < 2\pi$ as shown in Figs. 2(a). In contrast, WPA theorem states that formation of 2π pulse in the single-mode waveguide is possible only for $\Theta_p(0) > 2\pi n$ with $n \in \{1, 2, \dots\}$.

The former fact is simply explained by asymptotical behavior of the pulse area. For the initial pulse area within a range $2n\pi < \Theta_p(0) < 2(n+1)\pi$ the derivative becomes negative $\frac{\partial}{\partial z} \Theta_p(z) < 0$ that results in asymptote $T_0(\Theta_p(z) \gg \varkappa_1^{-1}) \rightarrow \ln[\Theta_p(z)/2]$. According to Eq. (40), for $n = 0$ the pulse area evolves asymptotically

$$\Theta_p(z \gg \varkappa_1^{-1}) \cong e^{T_0(\Theta_p(0)) - \varkappa_1 z/2} \rightarrow 0, \quad (41)$$

while for $n = 1, 2, \dots$,

$$\Theta_p(z \gg \varkappa_1^{-1}) \cong 2\pi n \left(1 + \frac{1}{\frac{\varkappa_1 z}{2} - T_n(\Theta_p(0))} \right) \rightarrow 2\pi n. \quad (42)$$

Remarkably, the asymptote of $\Theta_p(z \gg \varkappa_1^{-1})$ for $n \neq 0$ does not have an exponential character and slowly converges compared to the solution $\Theta_p(z \gg \varkappa_1^{-1})$ for $n = 0$. Similarly, the formation of 2π pulse in the waveguide occurs at almost 10-fold larger optical depth than for plane wave as depicted in Figs. 2(a) and 2(b). The formation of the second and subsequent 2π pulses in the waveguide is also shifted into region of larger optical depth. One reason for that is the weaker interaction between the waveguide mode and atoms away from the center of the waveguide. In principle, this reduction may be compensated by an effective increase of the coupling constant via the decreased group velocity of the light modes $v_g \ll c$ [see comments to (31)] and stronger mode confinement in the waveguide.

For the pulse areas close to $2\pi n$, attenuation will be caused only by nonresonant losses with $\Theta(z) \approx 2\pi n \exp\{-\frac{\gamma_w z}{2v_g}\}$. Such pulses will persist the longest solitonlike propagation for weak nonresonant losses ($\frac{\gamma_w z}{2v_g} \ll 1$). However, at large deviations of the signal pulse area from $2\pi n$ the contribution of resonant interaction in bringing the pulse area to $2\pi(n-1)$ becomes dominant. Such an evolution is to be repeated until the light field is completely absorbed.

The presence of several different dipole moments \mathbf{d}_m and, accordingly, different pulse areas $\Theta_{m,p}$ significantly change the behavior of the pulse area. The formation of relatively stable 2π pulses becomes possible, probably, only if the condition $\Theta_{m,p} = 2n\pi$ is met for each atomic group m . A detailed study of the implementation of such scenarios for the formation of 2π pulses is beyond the scope of the current analysis.

III. MULTIPULSE EXCITATION AND ECHO SIGNAL EMISSION

A. Pulse-area theorem of echo signal in single-mode waveguide

Here we apply the WPA theorem to the description of the photon echo in an ensemble of two-level atoms uniformly distributed in the volume of a single-mode waveguide. We assume that the signal pulse is launched at time $t = 0$ and its interaction with two-level atoms is governed by WPA theorem that is described in Sec. II. After signal an additional control pulse with a delay of τ is applied to the medium. The delay is assumed to be much longer than the signal pulse duration ($\tau \gg \delta t$).

The signal pulse affects on the initial atomic population $w_{m,s}(\mathbf{r}_\perp, z)$ that changes the initial conditions in the equation for the envelope area of the control pulse. With the help of Eqs. (19)–(22), Eq. (29) is modified accordingly to reflect the initial atomic population

$$\left(\frac{\partial}{\partial z} + \frac{\gamma_w}{2v_g} \right) \theta_1 = \sum_{m=1}^M \frac{\xi_m}{2} \int_S dx dy \Omega_{0,m}(\mathbf{r}_\perp) w_{m,s}(\mathbf{r}_\perp, z) \times \sin[\Theta_{m,1}(\mathbf{r}_\perp, z)], \quad (43)$$

where $w_{m,s}(\mathbf{r}_\perp, z) = -\cos[\Theta_{m,s}(\mathbf{r}_\perp, z)]$, $\Theta_{m,s}(\mathbf{r}_\perp, z) = \Omega_{0,m}(\mathbf{r}_\perp)\theta_s(z)$ is the pulse area of the signal pulse for an atom located at the point (\mathbf{r}_\perp, z) . The pulse area of signal can be expressed by previously derived (39) for Gaussian-type membrane function.

Next, we derive an equation for the envelope area $\theta_e(z)$ of the simple two-pulse (primary) echo. Following the same procedure as with derivation of WPA theorem we integrate the equation for the field amplitude over time. The echo is expected at $t = 2\tau$, thus, the integration is reasonable to start from the moment of time before the echo at $t = 3\tau/2$ and finish after echo irradiation $t = 5\tau/2$: $\theta_e(z) = \int_{3\tau/2}^{5\tau/2} dt a_e(z, t)$. Since the echo signal is time separated from other light pulses, we carry out the integration as in Sec. II and take into account the initial atomic polarization that results in the following equation for the envelope area θ_e of the echo pulse:

$$\begin{aligned} & \left(\frac{\partial}{\partial z} + \frac{\gamma_w}{2v_g} \right) \theta_e \\ &= \sum_{m=1}^M \frac{\xi_m}{2} \int_S dx dy \Omega_{0,m}(\mathbf{r}_\perp) \\ & \times \left\{ 2\Gamma(\mathbf{r}, \tau, \dots) P_m(\mathbf{r}_\perp, z) \cos^2 \left(\frac{1}{2} \Theta_{m,e}(\mathbf{r}_\perp, z) \right) \right. \\ & \left. + w_m(\mathbf{r}_\perp, z) \sin[\Theta_{m,e}(\mathbf{r}_\perp, z)] \right\}, \end{aligned} \quad (44)$$

where $\Theta_{m,e}(\mathbf{r}_\perp, z) = \Omega_{0,m}(\mathbf{r}_\perp)\theta_e(z)$, $P_m(\mathbf{r}_\perp, z)$ is the source of the echo being the phasing part of the polarization of the m th atomic ensemble taken at the central frequency, $w_m(\mathbf{r}_\perp, z)$ is the nonoscillating part of the population of m th atomic ensemble at the central frequency [9,46,47]. Note that in the case of plane waves $f(\mathbf{r}_\perp) = 1$ and $\gamma_w = 0$, the analytical solution of Eq. (44) for $M = 1$ is found using substitution $\theta_e(z) = \frac{2}{\Omega_0} \arctan u(z)$. This solution shows that the pulse area of each echo signal $\Theta_e = \Omega_0\theta_e(z)$ does not exceed π and decreases to zero at high optical depth [9].

The term $\Gamma(\mathbf{r}, \tau, \dots)$ describes the phase relaxation in the interval between signal pulse and echo pulse. As previously, the influence of phase relaxation during the relatively short interaction time between light pulses and the polarization is neglected for a simple integration [9]. At the same time, the phase relaxation in the interval between the pulses and the echo pulse is included. For sake of simplicity, the exponential relaxation factors $\Gamma(\dots) = e^{-(2\tau/T_M)^x}$ for primary echo and $e^{-(2\tau/T_M)^x}$ for ROSE signal are used [60], where x is the fitting power factor. It should be emphasized that various decoherence mechanisms, particularly depending on the level of atom excitation, may require specific study. One such mechanism is the effect of instantaneous spectrum diffusion [61,62].

B. Pulse area of two-pulse (primary) photon echo and all subsequent echoes

Below we analyze the solution of Eq. (44) for the two-pulse (primary) echo and the pulse area of all subsequently induced echoes in an optically dense two-level medium under the assumption of weak phase relaxation [$\Gamma(\mathbf{r}, \tau, T_M, \Theta_{s,1}, \beta) = 1$]. First, we consider the case of two copropagating pulses as illustrated in Fig. 4(a). The initial conditions of the

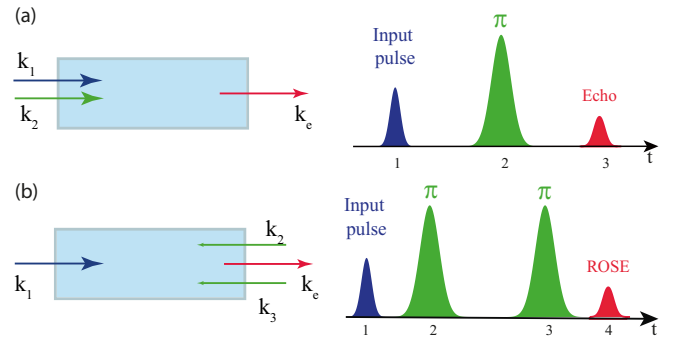


FIG. 4. Spatial schemes and temporal sequences of light pulses in (a) the primary echo, (b) the revival of silenced echo (ROSE) protocol.

envelope equation contain the components of atomic inversion $w_m(\mathbf{r}_\perp, z) = w_m^{pe}(\mathbf{r}_\perp, z)$ and coherence $P_m(\mathbf{r}_\perp, z) = P_m^{pe}(\mathbf{r}_\perp, z)$, which are expressed as

$$\begin{aligned} w_m^{pe}(\mathbf{r}_\perp, z) &= -\cos[\Theta_{m,s}(\mathbf{r}_\perp, z)] \cos[\Theta_{m,1}(\mathbf{r}_\perp, z)], \\ P_m^{pe}(\mathbf{r}_\perp, z) &= \sin \Theta_{m,s}(\mathbf{r}_\perp, z) \sin^2 \left(\frac{1}{2} \Theta_{m,1}(\mathbf{r}_\perp, z) \right). \end{aligned} \quad (45)$$

The only difference between the expressions in Eqs. (45) and similar solutions for a plane wave [9,46] is the dependence of the pulse areas on the transverse coordinate \mathbf{r}_\perp . We integrate the atomic response along the transverse plane of the waveguide in the same way as in Eq. (33). The resulted equation for the envelope area of echo pulse is

$$\begin{aligned} \left(\frac{\partial}{\partial z} + \frac{\gamma_w}{2v_g} \right) \theta_e &= \sum_{m=1}^M \frac{\varkappa_m}{\Omega_m} \left\{ \frac{\Gamma(\tau, T_M, \dots)}{2} I_{s,m}(\theta_s, \theta_1, \theta_e) \right. \\ & \left. - S_m(\theta_e; \theta_s; \theta_1) \right\}, \end{aligned} \quad (46)$$

where

$$\begin{aligned} I_{s,m}(\theta_s, \theta_1, \theta_e) &= \frac{\sin^2(\Omega_m\theta_s/2)}{\Omega_m\theta_s/2} + S_m(\theta_s; \theta_e) \\ & - S_m(\theta_s; \theta_1) - S_m(\theta_s; \theta_1; \theta_e), \end{aligned} \quad (47)$$

$$S_m(\theta_p; \theta_q) = \frac{1}{2} \sum_{n=1}^2 \frac{\sin^2 \{ \Omega_m[\theta_p + (-1)^n\theta_q]/2 \}}{\Omega_m[\theta_p + (-1)^n\theta_q]/2}, \quad (48)$$

$$\begin{aligned} S_m(\theta_p; \theta_q; \theta_r) &= \frac{1}{4} \sum_{n=1}^2 \sum_{l=1}^2 \frac{\sin^2 \{ \Omega_m[\theta_p + (-1)^n\theta_q + (-1)^l\theta_r]/2 \}}{\Omega_m[\theta_p + (-1)^n\theta_q + (-1)^l\theta_r]/2}. \end{aligned} \quad (49)$$

For a single dipole moment type the resulted pulse areas of the input signal pulses $\Theta_s(z)$, control pulse $\Theta_1(z)$, primary echo $\Theta_e(z)$, and the total pulse area of all echoes $\Theta_{\Sigma,e}$ are depicted in Fig. 5. As seen in Figs. 5(a) and 5(b), the pulse area of the primary echo pulse $\Theta_e(z)$ experiences growth reaching its maximum and then decreasing to zero. The pulse area of the all echoes $\Theta_{\Sigma,e}(z)$ is defined as the difference between the total pulse area $\Theta_\Sigma(z)$ and individual pulse areas of the signal and control pulses $\Theta_s(z)$, $\Theta_1(z)$ as in [8], where the evolution

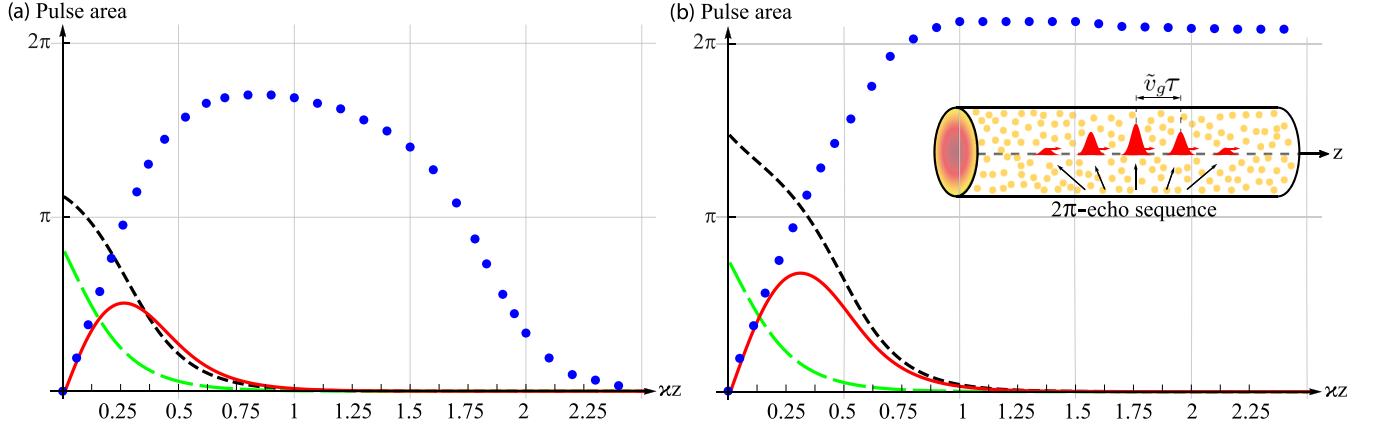


FIG. 5. Pulse areas for single atomic group $M = 1$ of signal pulse $\Theta_s(z)$ (green dashed line), first control pulse $\Theta_1(z)$ (black short dashed line), primary echo $\Theta_e(z)$ (red solid line), and all echo pulses $\Theta_{\Sigma,e}(z)$ (blue dotted line). (a) $\Theta_s(0) + \Theta_1(0) < 2\pi$, (b) $2\pi < \Theta_s(0) + \Theta_1(0) < 4\pi$. Inset conceptually illustrates formation of an 2π -echo sequence in the waveguide at some moment of time with total pulse area $\Theta_{\Sigma,e} = 2\pi$, where τ is a time interval between the two exciting pulses, \tilde{v}_g is a group velocity weakened by the light interaction with two-level atoms.

of total pulse area $\Theta_{\Sigma}(z)$ is described by Eq. (36) with initial pulse area $\Theta_{\Sigma}(0) = \Theta_s(0) + \Theta_1(0)$.

Figure 5(a) shows that if the initial total area $\Theta_{\Sigma}(0)$ is less than 2π , then the pulse area of all echo signals $\Theta_{\Sigma,e}(z)$ tends to zero at large optical depth $z \gg 1/\kappa$. In contrast, if $\Theta_{\Sigma}(0) > 2\pi$, then the pulse area of all echo signals $\Theta_{\Sigma,e}(z \gg 1/\kappa)$ tends to 2π , as it is seen in Fig. 5(b). This behavior does not coincide with the prediction of McCall-Hahn area theorem, where the threshold of the total area is π for the 2π pulse formation [see Fig. 2(a)]. It is also seen in Figs. 5(a) and 5(b) that in both the cases the primary echo amplitude increases with the optical density approaching its maximum without reaching to 2π . At large value of optical depth the primary echo gradually decays to zero. The growth of the pulse area to its maximum and its subsequent attenuation to zero is valid for each of the subsequent echoes, which is a common property of WPA theorem and free space theory [46,47]. The total pulse area is the sum of the pulse areas of several echo signals generated sequentially in a medium since total pulse area of all pulses tends to 2π , if $\Theta_{\Sigma}(0) > 2\pi$. Thus, the sequence of generated echoes in a single-mode waveguide behaves as a single 2π pulse, as in case with plane waves [9] and we indicate it in Fig. 5(b) as a 2π -echo sequence (see also discussion in Appendix A about the 2π -pulse excitation in a single-mode waveguide).

Following the approach [9,10] and using one-dimensional Eq. (44) with corresponding expressions for the phasing polarization and initial atomic inversion, it is also possible to get equations for an envelope area of an arbitrary echo signal, which can be easily solved numerically. Below, we developed photon echo WPA theorem to the photon echo in ROSE protocol [35,43,63].

IV. ROSE PROTOCOL IN A LASER-WRITTEN WAVEGUIDE CRYSTAL

A. Waveguide pulse-area equation of ROSE signal

ROSE is echo protocol for quantum storage being closest to the convectonal two-pulse echo. If implemented properly,

it suppresses unwanted quantum noise that appears at primary echo emission. The spatial and temporal schemes of ROSE protocol are shown in Fig. 4(b). In ROSE protocol a two-level medium is first excited by a weak signal pulse at time $t = 0$. Two π pulses are applied to medium at $t = \tau$ and 3τ that forms an echo at $t = 4\tau$. The control pulses should propagate in the opposite direction with respect to the direction of the signal pulse to mitigate generation of the primary photon echo.

For signal, echo, first, and second π pulses we use indices $(s, e, 1, 2)$, respectively. The pulse area after the weak signal and first π pulse are described by Eqs. (39) and (40) (where to make replacements: $z \rightarrow (L - z)$ and $\theta_1(0) \rightarrow \theta_1(L)$), due to negligibly small pulse area of the signal. Since the first control pulse has a pulse area close to π it strongly affects the propagation of the second control pulse ($p = 2$). In this case, similarly to [8], we get the following equation for the envelope area θ_2 of the second control pulse:

$$\left(-\frac{\partial}{\partial z} + \frac{\gamma_w}{2v_g}\right)\theta_2 = -\sum_{m=1}^M \frac{\xi_m}{2} \int_S dx dy \Omega_{0,m}(\mathbf{r}_{\perp}) \times \cos[\Theta_{m,1}(\mathbf{r}_{\perp}, z)] \sin[\Theta_{m,2}(\mathbf{r}_{\perp}, z)]. \quad (50)$$

By using Gaussian membrane function in Eq. (50) and performing the calculation similar to the derivation of Eqs. (33) and (46), we get

$$\left(-\frac{\partial}{\partial z} + \frac{\gamma_w}{2v_g}\right)\theta_2 = -\sum_{m=1}^M \frac{\varkappa_m}{\Omega_m} S_m(\theta_2; \theta_1), \quad (51)$$

where $S_m(\theta_p; \theta_q)$ is given in Eq. (49). For the particular case of weak second control field ($\Omega_m \theta_2 \ll \pi$), Eq. (51) transforms into the linear equation for θ_2 :

$$\left(-\frac{\partial}{\partial z} + \frac{\gamma_w}{2v_g}\right)\theta_2(z) = -\frac{1}{2} \sum_{m=1}^M \varkappa_m [\Theta_{m,1}(z)] \theta_2, \quad (52)$$

where $\varkappa_m(\Theta_{m,1}(z))$ is a changed absorption coefficient of m th atomic group [$\Theta_{m,1}(z) = \Omega_m \theta_1(z)$]:

$$\varkappa_m[\Theta_{m,1}(z)] = \varkappa_m \left\{ 2 \frac{\sin[\Theta_{m,1}(z)]}{\Theta_{m,1}(z)} - \frac{\sin^2[\Theta_{m,1}(z)/2]}{[\Theta_{m,1}(z)/2]^2} \right\}, \quad (53)$$

where $\varkappa_m(\Theta_{m,1} \rightarrow 0) = \varkappa_m$ and $\varkappa_m(\Theta_{m,1}) < 0$ for $\tan(\Theta_{m,1}/2) > \Theta_{m,1}$, i.e., for $\Theta_{m,1} > 2.3311$. In this condition the second control pulse is amplified, if nonresonant losses are weak, $\gamma_w L \ll 1$. If $\Theta_2(0) < 2\pi$, the amplification of second pulse $\Theta_2(z)$ is replaced by its attenuation to zero at large optical depth $z \gg 1/\varkappa$. As in the case of the primary echo, the pulse area of ROSE protocol $\Theta_e(z)$ experiences growth to a maximum and decrease to zero at large value of optical depth. The evolution of the envelope area $\theta_e(z)$ in ROSE sequence is described by Eq. (44), where the initial atomic population $w_m(\mathbf{r}_\perp, z) = w_m^{re}(\mathbf{r}_\perp, z)$ and phasing coherence $P_m(\mathbf{r}_\perp, z) = P_m^{re}(\mathbf{r}_\perp, z)$ are [44]

$$\begin{aligned} w_m^{re}(\mathbf{r}_\perp, z) &= \cos[\Theta_{m,s}(\mathbf{r}_\perp, z)] \prod_{p=1}^2 \cos[\Theta_{m,p}(\mathbf{r}_\perp, z)] \\ &\cong -\cos[\Theta_{m,1}(\mathbf{r}_\perp, z)] \cos[\Theta_{m,2}(\mathbf{r}_\perp, z)], \\ P_m^{re}(\mathbf{r}_\perp, z) &\cong \Omega_{0,m}(\mathbf{r}_\perp) \theta_s(0) e^{-\alpha z/2} \prod_{p=1}^2 \sin^2 \left(\frac{1}{2} \Theta_{m,p}(\mathbf{r}_\perp, z) \right), \end{aligned} \quad (54)$$

where $\cos[\Theta_{m,s}(\mathbf{r}_\perp, z)] \cong 1$ and

$$\sin \Theta_{m,s}(\mathbf{r}_\perp, z) \cong \Theta_{m,s}(\mathbf{r}_\perp, z) = \Omega_{0,m}(\mathbf{r}_\perp) \theta_s(0) e^{-\alpha z/2}, \quad (55)$$

with pulse areas $\Theta_{m,p}(\mathbf{r}_\perp, z) = \Omega_{0,m}(\mathbf{r}_\perp) \theta_p(z)$ ($p = 1, 2$) being close to π for highly efficient quantum memory ROSE protocol. In the studied counterpropagating geometry “ $\frac{\partial}{\partial z}$ ” should be replaced by “ $-\frac{\partial}{\partial z}$ ” in Eqs. (33) and (43), when considering the second control pulse [see Eqs. (50), (51), and (52)]. At the same time, the efficiency of echo signal retrieval does not depend on the direction of its radiation due to the low optical density.

We note that $\theta_s, \theta_1, \theta_2$ in (44), (45), (54) can be found according to Eqs. (33) and (43) for the forward and backward propagation of the control pulses (with replacement “ $\frac{\partial}{\partial z}$ ” by “ $-\frac{\partial}{\partial z}$ ”). Similar as with Eqs. (52) and (53), we find that the absorption coefficients $\varkappa_m[\Theta_1(z); \Theta_2(z)]$ in (B6) can be positive or negative, thereby leading to absorption or amplification of the echo signal. The last case is not suitable for QM due to quantum noise in the echo signal. For generality, in Appendix B, we provide equations for the pulse area of ROSE echo signal for arbitrary intensities of the signal and control fields in the waveguide with optically dense medium.

In our experiment, both control laser pulses have phase and amplitude modulations [44] that provide a uniform spectral and spatial excitation of atoms in the central part of the waveguide cross section, allowing a significant increase in the efficiency of the echo’s signal emission.

B. Experimental setup

We implement ROSE protocol in the waveguide that being laser written in $\text{Tm}^{3+}:\text{Y}_3\text{Al}_5\text{O}_{12}$ crystal with Tm^{3+} doping

of 0.01% and dimensions $2 \times 9 \times 19.5$ mm. The crystal is one of the well-known crystals, convenient for testing and development of optical QM protocols [44,64]. Simplified experimental setup is depicted in Fig. 6(a). Laser light from a single-mode fiber is coupled into a single waveguide by an objective (Edmund Optics ELWD 10 \times 59877) on one side and an aspheric lens (Thorlabs A280TM-B) installed in a cryostat from another side of the crystal with an efficiency of 30%. Light is detected by an avalanche photodetector (APD, Thorlabs APD120A/M) connected to an oscilloscope (Tektronix DPO7104C) or a single-photon counting module (SPCM, Excelitas SPCM-AQRH). The crystal is glued with silver paste to a cold finger and placed in a closed-cycle cryostat (Montana Instruments Corp.) with a temperature of 3.2 ± 0.1 K. Crystallographic axes of the crystal are oriented with respect to crystal edges, as it is shown in the inset of Fig. 6(a), where $\alpha_E = 11.3^\circ$, $\beta_E = 4.3^\circ$, and $\gamma_E = 0^\circ$ are conventional Euler rotation angles.

The type-III depressed cladding single-mode waveguides were produced by a femtosecond laser writing technique in $\text{Tm}^{3+}:\text{Y}_3\text{Al}_5\text{O}_{12}$ crystal [45]. Each waveguide is composed of 18 elliptical tracks with axes of 2 and 8 μm around a core with diameter of 18 μm . The femtosecond laser pulses change the refractive index of the elliptical tracks by $\sim 10^{-3}$ that confines the light within the inner core. Propagation losses for vertical polarization (parallel to 2 mm edge of the crystal) is 0.66 dB/cm, for horizontal polarization (parallel to 9 mm edge) is 1.13 dB/cm. Totally 20 one type-III single-mode waveguides have been written in the crystal along Z axis. Since the exact difference in refractive index Δn is unknown, we perform finite-difference time-domain simulation of the eigenmodes for different values of Δn [65]. If $\Delta n > 2 \times 10^{-3}$ the waveguide supports symmetrical Gaussian mode with half-width at half-maximum of ~ 5.5 μm for both axes as shown in Fig. 6(b). At lower values of Δn the mode becomes elliptical with the widths for orthogonal axes being different more than two times. At the same time, the experimentally measured modes have symmetrical Gaussian character that witnesses the actual width of the waveguide mode to be ~ 5.5 μm . Hence, further on we assume the width of $a = 5.5$ μm in membrane function $f_g(\mathbf{r}_\perp)$.

It should be noted that recent studies have conducted experiments on the implementation of photon echo AFC protocol in waveguides fabricated by the same technology [16,18,33–35]. Whereas the cited publications used type I, type II, and type IV waveguides, we present type III waveguides in this work. The advantage of type III waveguide is a support of arbitrary polarization in a waveguide mode.

The continuous wave titan-sapphire laser (Tekhnoscan TIS-SF-777) is tuned to $^3\text{H}_6(0) \rightarrow ^3\text{H}_4(0)$ optical transition of Tm^{3+} ($\lambda \approx 793.365$ nm). Two acousto-optic modulators (AOMs) are used to sample microsecond-scale pulses for performing primary echo measurements and the ROSE protocol. The outputs of AOMs are spatially filtered by single-mode fibers and sent parallel to the long edge of the crystal (19.5 mm) in counterpropagating geometry. The linearly polarized signal is routed via 50:50 beam splitter to the APD for intensity monitoring as a reference and to the crystal, as shown in Fig. 6(a). After passing through the quarter-wave plate the beams are circularly polarized.

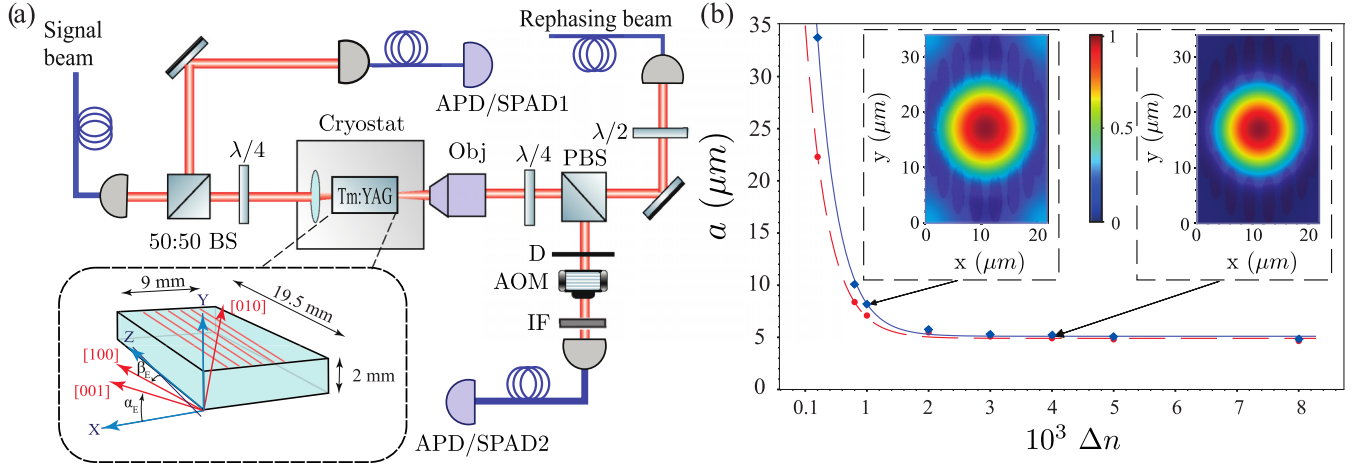


FIG. 6. (a) Simplified experimental scheme, where IF is an interference filter, Obj is an objective, also there is one more objective installed inside the cryostat on the left side of the crystal, D is a diaphragm, AOM is an acousto-optic modulator, BS is nonpolarizing beam splitter, PBS is polarizing beam splitter, $\lambda/4$ is quarter-wave plate, $\lambda/2$ is half-wave plate, APD is an avalanche photodiode, SPAD is a single-photon avalanche photodiode, $\alpha_E = 11.3^\circ$, $\beta_E = 4.3^\circ$ are conventional Euler rotation angles. (b) Simulated full width at half-maximum a of the laser-written waveguide eigenmode at different values of the refractive index contrast $10^{-4} < \Delta n < 8 \times 10^{-3}$ between the elliptical tracks and the core. The red dashed and blue solid curves correspond to widths along two orthogonal axes x and y , respectively. Two inserts show the color map of normalized spatial distribution of the eigenmode's intensity for $\Delta n = 10^{-3}$ and $\Delta n = 4 \times 10^{-3}$.

Tm³⁺ ions substitute yttrium ions in six ($M = 6$) crystallographically equivalent but orientationally inequivalent sites of Y₃Al₅O₁₂ crystal. The light beams with circular polarization interact with all these sites. The Rabi frequency of optical transition $\Omega_m = E_0 \langle \mathbf{d}_m \cdot \mathbf{e} \rangle / \hbar$ is larger for the third and fourth sites. In order to make the pulse area of the control pulses to be close to π for the atoms in wider spectral range, we use phase-modulated control laser pulses. The theoretical modeling of the control pulse Rabi frequencies and phase modulation is given by the relations (see also Appendix B)

$$\Omega_m(\tau, \mathbf{r}_\perp) = \Omega_{m,1}(\tau - t_1, \mathbf{r}_\perp) + \Omega_{m,2}(\tau - t_2, \mathbf{r}_\perp), \quad (56)$$

where

$$\Omega_{m,p}(\tau - t_1, \mathbf{r}_\perp) = \dot{A}_{m,p}(\tau - t_1, \mathbf{r}_\perp) e^{-iB_p(\tau - t_p)}, \quad (57)$$

$$\dot{A}_{m,p}(t, \mathbf{r}_\perp) = \frac{\chi_{m,p}(\mathbf{r}_\perp)}{\pi \delta t_p} \frac{e^{-i\varphi_p}}{\cosh(t/\delta t_p)}, \quad (58)$$

$$\dot{B}_p(t) = \Delta + \frac{\beta_p}{\pi \delta t_p} \tanh(t/\delta t_p), \quad (59)$$

where $\tau = t + z/v_g$, $\chi_{m,p}(\mathbf{r}_\perp) = \chi_{0,m,p} f_g(\mathbf{r}_\perp/a)$.

The parameters of the control pulses negligibly change in an optically thin medium, so that we can approximate the Rabi frequency of the control fields: $\Omega_{m,p}(\mathbf{r}, t) = \Omega_{0,m}(\mathbf{r}_\perp) a_p(t + z/c)$ [where $p = 1, 2$, $a_p(t + z/v_g) = \langle \hat{a}_p(z, t) \rangle$ is a classical value]. The maximum CW optical power of the control beam before cryostat is 9 mW. The parameters β_p and δt_p are responsible for the frequency sweep range and the pulse duration, respectively and are chosen in the range $\beta_p/\pi = 1-7$ and $(2\pi \delta t_p)^{-1} = 140-400$ kHz. The input pulse, its transmitted portion, and the ROSE signal are measured by APD/SPAD1 and APD/SPAD2, respectively, as shown in Fig. 6(a).

Figures 7(a) and 7(b) show the experimental data on the storage of the weak input light pulse with the waveguided ROSE protocol. Timing of the input signal, two control pulses,

and the echo is presented in Fig. 7(a). The input signal light pulse with Gaussian waveform and full width at half-maximum duration of 1 μ s is launched at $t = 0$. The rephasing pulses are shown at $t = 7.5 \mu$ s and $t = 22.5 \mu$ s measured by a detector in the reference channel of rephasing beam. The recovery efficiency 0.5% of the input pulse is achieved for a storage time of 30 μ s. It should be noted that for the used geometry, the absorption value $\alpha L = 0.12$ and the coherence time of the optical transition $T_M = 63 \mu$ s ($x = 1.82$), the maximum efficiency of the ROSE pulse is limited by $\eta_{\max} = (\alpha L)^2 e^{-\alpha L} e^{-2(4\tau/T_M)^x}$ (with 4τ being the storage time), bearing in mind two ideal control π light pulses. According to this estimation, the maximum achievable efficiency in our optically thin crystal is $\eta_{\max} = 0.76\%$. Below we analyze the experimental data obtained for the ROSE protocol in a waveguide using (44), (54), and (55) taking into account the experimental parameters of the medium, signal pulses, and modeling the parameters of the control pulses by Eqs. (56)–(59).

C. Theoretical discussion of experimental results

In our experiment, the inhomogeneous broadening of the resonant optical transition is larger than the spectrum of the control pulses ($\Delta_{\text{in}} \gg \delta\omega_{1,2}$, see also Fig. 1), and the spectrum width of the signal pulse was even smaller ($\delta\omega_s \approx \delta t_s^{-1} < \delta\omega_{1,2}$). As depicted in Fig. 7(a), in this regime the temporal shape of the echo signal reproduces the temporal shape of the signal pulse. Hence, the realized protocol fulfills spectral conditions for the efficient implementation of the photon echo QM [41,66,67]. The reproduction of temporal profile in the echo allows to apply the pulse-area approach with Eqs. (44), (45), and (54) to describe the basic patterns of the realized ROSE protocol.

For a negligibly weak pulse area of the input signal pulse the probability of exciting the atoms \mathcal{P}_{11} after the first chirped

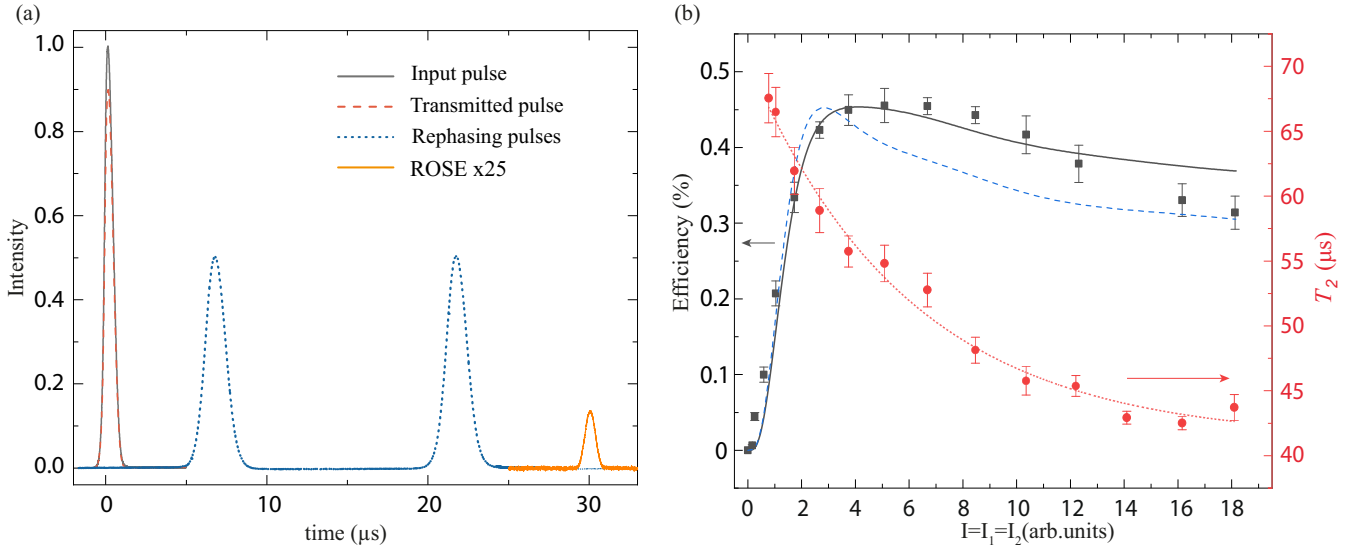


FIG. 7. (a) The signal of the revived silenced echo magnified by 25 is shown at time 30 μs (orange curve) obtained in the waveguide in $\text{Tm}^{3+}:\text{Y}_3\text{Al}_5\text{O}_{12}$ crystal. The rephasing pulses are shown by the blue dotted curve. At $t = 0$, μs input pulse and transmitted part are shown by black and red dashed curves, respectively. (b) The retrieval efficiency of input pulse (black squares) and effective coherence time T_2 of optical transition (red circles) of the waveguide optical memory versus intensity of two identical rephasing pulses $I = I_1 = I_2$. The theoretical fits with Eq. (65) (black solid line) and plane-wave theory (blue dashed line) are presented.

pulse ($p = 1$) is calculated using the analytical solution [68] (see also Appendix C):

$$\sin^2\left(\frac{1}{2}\tilde{\Theta}_{m,p}(\mathbf{r}_\perp)\right) = \sin^2\left(\frac{1}{2}\Phi_{m,p}(\mathbf{r}_\perp)\right) + \cos^2\left(\frac{1}{2}\Phi_{m,p}(\mathbf{r}_\perp)\right) \times \tanh^2\left(\frac{\beta}{2}\right), \quad (60)$$

where $\tilde{\Theta}_{m,p}(\mathbf{r}_\perp)$ is an effective pulse area of chirped pulse for resonant atoms ($\Delta = 0$), $p = 1, 2$, $\Phi_{m,p}(\mathbf{r}_\perp) = [\chi_{m,p}^2(\mathbf{r}_\perp) - \beta^2]^{\frac{1}{2}}$ with the same chirping being used for both control pulses $\beta_p = \beta$.

Assuming negligible change in the parameters of the control laser pulses in the optically thin medium, Eq. (44) is adopted for the envelope area of the echo θ_e :

$$\left(\frac{\partial}{\partial z} + \frac{\gamma_w}{2v_g}\right)\theta_e = \sum_{m=1}^M \frac{\xi_m}{2} \int_S dx dy \Omega_{0,m}(\mathbf{r}_\perp) \times \{2\Gamma(\mathbf{r}, \tau, T_M, \Theta, \beta)P_m(\mathbf{r}_\perp, z) + w_m(\mathbf{r}_\perp, z)\Omega_{0,m}(\mathbf{r}_\perp)\theta_e\}, \quad (61)$$

where $P_m(\mathbf{r}_\perp, z)$ and $w_m(\mathbf{r}_\perp, z)$ are given in Eqs. (54) and (55) (see also Appendix C), $\Gamma(\mathbf{r}, \tau, T_M, \Theta, \beta) = e^{-(4\tau/T_M)^x} \exp\{-2\frac{\tau}{T_s(\mathbf{r}_\perp, \Theta, \beta)}\}$ characterizes the phase relaxation of resonant atoms located in a cross section of the waveguide with a coordinate \mathbf{r}_\perp ; an additional phase relaxation time $T_s(\mathbf{r}_\perp, \Theta, \beta)$ is determined by the relaxation processes depending on the location of the atom in the waveguide (pulse areas Θ and β determine the degree of atomic excitation in all atomic groups $m = 1, \dots, M$).

To study the echo pulse area with Eq. (61), it is necessary to independently determine the phase relaxation factor $\Gamma(\mathbf{r}, \tau, T_M, \Theta, \beta)$. The properties of $\Gamma(\mathbf{r}, \tau, T_M, \Theta, \beta)$ are extracted from experimentally measured dependence of the

ROSE signal decay at different intensity of the control pulses. The obtained results show that the effective phase relaxation time T_s of the ROSE signal depends on the intensity of the control pulses, as depicted by the red circles in Fig. 7(b). We fit the dependence of effective relaxation time $T_s(I, \beta)$ (red dotted line in this figure) on the intensity I of the control pulses at the given phase modulation β . The intensity of the control pulses reduces the phase relaxation time of the optical coherence by about 1.5 times (from 67 to 42 μs) for the concentration of Tm^{3+} 0.01 at.%, which is an order of magnitude less than in the well-known experiments [62], where the additional attenuation of the echo signal is explained by the influence of the spectral diffusion effect observed earlier.

Taking into account the obtained experimental data, we limit ourselves to the effective constant of phase relaxation $1/T_s(I, \beta)$. Determination of the phase relaxation time $T_s(\mathbf{r}_\perp, \Theta, \beta)$ requires the a more detailed theory that takes into account the features of phase relaxation in an optical waveguide, the inhomogeneous distribution of the intensity of the control fields and the additional experiments, which is beyond the scope of this work and will be carried out somewhere else. It is also worth noting that the created waveguides remain imperfect and it will be necessary to take into account the influence of the defects created in them. At the same time, we note that the defects that appear in the waveguide do not dramatically reduce the phase relaxation time [69], which preserves the hope for further use of the waveguides under study.

If the parameters of the two control laser pulses are identical $\tilde{\Theta}_{m,2}(\mathbf{r}_\perp, z) = \tilde{\Theta}_{m,1}(\mathbf{r}_\perp, z)$, the solution of (61) is

$$\theta_e(z, \xi, \tau) = 2 \frac{e^{-(4\tau/T_M)^x} A_w(I, \Theta, \xi, \tau) \theta_s(0)}{(\alpha_w - \alpha)} \times (e^{-\frac{1}{2}\alpha z} - e^{-\frac{1}{2}\alpha_w z}), \quad (62)$$

where $A_w(I, \Theta, \xi, \tau) = \sum_{m=1}^M A_{0,m}(I, \Theta, \xi, \tau)$, $\alpha_w = \gamma_w + \sum_{m=1}^M \varkappa_{m,w}$ is an absorption coefficient for echo pulse:

$$\varkappa_{m,w} = \frac{\xi_m}{2} \int_S dx dy \Omega_{0,m}^2(\mathbf{r}_\perp) \cos^2[\tilde{\Theta}_{m,1}(\mathbf{r}_\perp)], \quad (63)$$

$$A_{0,m}(I, \Theta, \xi, \tau) = \xi_m \exp\left\{-\frac{2\tau}{T_s(I, \beta)}\right\} \int_S dx dy \Omega_{0,m}^2(\mathbf{r}_\perp) \times \sin^4\left(\frac{1}{2}\tilde{\Theta}_{m,1}(\mathbf{r}_\perp)\right), \quad (64)$$

where $A_{0,m}(I, \Theta, \xi, \tau)$ describes the averaged over the waveguide cross-section response of m th atomic group, which contributes to the amplitude of ROSE signal and $A_w(I, \Theta, \xi, \tau)$ gives a total response from all the atomic groups. Remarkably, the observed averaged phase relaxation factor $\exp\{-\frac{2\tau}{T_s(I, \beta)}\}$ in Eq. (64) leads to nonexponential temporal decay. From Eq. (62), we get for the envelope area θ_e at the crystal output ($z = L$) in optically thin atomic ensemble ($\alpha L \ll 1$, $\alpha_w L \ll 1$)

$$\theta_e(L, I, \Theta, \xi, \tau) = e^{-(4\tau/T_M)^x} \theta_s(0) A_w(I, \Theta, \xi, \tau) L. \quad (65)$$

The function $A_w(I, \Theta, \xi, \tau)$ together with $e^{-(4\tau/T_M)^x}$ describes the influence of the transverse structure of the waveguide light modes, intensity, and chirping of control pulses, as well as the intensity-dependent phase relaxation $\exp\{-\frac{2\tau}{T_s(I, \beta)}\}$.

The experimental dependence of the ROSE signal on the intensity of two identical control laser pulses is presented in Fig. 7(b). The experimental data are satisfactorily fitted by $|\theta_e(L, I, \Theta, \beta, \tau, \delta t_p)|^2$ from Eq. (65) with $\beta/\pi = 7$, $\tau = 8.5$, $\delta t_p = 3$ and Gaussian membrane function with single type of atomic dipole moment. The relatively large value of $\beta/\pi = 7$ is the best fit to the experimentally realized envelope of the control pulses with their smaller central part of the pulses compared to its fronts. A similar theory for plane waves, i.e., of the uniform intensity in the cross section, is presented in Fig. 7(b). As it is seen from the comparison between the two theoretical curves, the echo signal for the control fields with a plane wave has sharper maximum. The echo signal then decreases faster due to the influence of phase relaxation that is proportional to the intensity of the control field. The experimentally observed echo signal has a longer plateau in the maximum region, which is consistent with the theoretical curve based on the WPA theorem. This behavior of the echo is apparently due to the compensation of growing phase relaxation by an increase in the number of atoms that are excited by π pulses in the cross section of the waveguide at larger intensities of the control pulses. The relatively small difference in the theoretical curves is also due to the weak phase relaxation.

We conclude that instantaneous spectral diffusion is mainly responsible for the drop in the efficiency of the echo signal. There is a slight difference between the experimental data and the theoretical dependence of echo on intensity of the control pulses. The difference may be attributed to a number of reasons, including an approximate description of the dependence of phase relaxation on the intensity of the control pulses. At the same, the quadratic dependence of the echo signal on intensity of the control pulses before the maximum indicates presence of phase modulation in control laser pulses.

V. CONCLUSION

In this work, we derive the waveguide pulse area (WPA) theorem for the interaction of light pulses with an inhomogeneously broadened two-level medium in a single-mode optical waveguide. We present an analytical solution to this theorem for a mode with a Gaussian intensity profile. Possibility of 2π -pulse formations for fundamental Gaussian and Gaussian-type (Bessel) light modes was shown. The formation of these 2π pulses and their main properties is compared to prediction of the McCall-Hahn area theorem [5]. The formation of 2π pulses in a single-mode fiber raises the question of the spatial-temporal structure of the resulting light pulses, which is the topic of special research.

Next, we develop the WPA theorem for studies of photon echo in the single-mode waveguide and apply it to analyze the two-pulse (primary) photon echo and the full sequence of generated echo signals after two-pulse excitation. It is possible to form a sequence of echo signals with a total pulse area of 2π . It coincides with the results obtained for the plane waves [8,9]. However, the initial total pulse area of the two exciting pulses should exceed 2π , and not π , as in the case with plane wave.

We use the WPA theorem for the description of the ROSE protocol in a single-mode waveguide and implement this protocol in an optically thin single-mode laser-written waveguide in $\text{Tm}^{3+}:\text{Y}_3\text{Al}_5\text{O}_{12}$ crystal. The observed recovery efficiency of input pulse for a storage time of 30 μs was 0.5% that corresponds to 65.7% of maximum possible value at given optical depth. In these experiments, we observed considerable influence of the control laser pulse's intensity on the phase relaxation of ROSE signal in a crystal with the lowest concentration 0.01% of Tm^{3+} ions in a $\text{Tm}^{3+}:\text{Y}_3\text{Al}_5\text{O}_{12}$ crystal. Despite the use of rephasing pulses with amplitude and frequency modulation, the retrieval efficiency still decreases with an increase in the control pulse's intensity.

The theoretical analysis with WPA theorem allows to satisfactorily explain the obtained experimental data. It was experimentally shown that the waveguide nature of the interaction between light fields and atoms manifests itself in an echo signal even for an optically thin atomic medium. The decrease in the echo signal with a growth in the intensity of the controlling laser pulses is explained by a decrease in the phase relaxation time, which could be explained by the effect of instantaneous spectral diffusion. In order to highly suppress the negative effect of instantaneous spectral diffusion for the implementation of QM on photon echo, one can use the crystals with even lower concentration of the atoms, which is necessary for the QM protocols in high-quality optical resonators [70]. It is worth noting that not only the presence of pure dephasing and instantaneous spectral diffusion [62,71] limits the efficiency of the ROSE protocol in the waveguide, but also the difficulties in achieving an ideal control laser π pulse providing uniform distribution of working atoms in the waveguide cross section. Fabrication of the waveguides with the active atoms within close proximity of waveguide mode's center is of a great interest for subsequent research.

The performed studies demonstrate the convenience of WPA theorem for describing nonlinear interaction, generation, and propagation of 2π pulses and the photon-echo-based

QM protocols in single-mode optical waveguides. Moreover, the developed approach may also be applied for studies of these effects in other waveguides. It is worth noting that practically all photon echo QM protocols can be implemented in a three-level media, where new opportunities appear for quantum processing with signal fields [72] and for developing new methods for generating quantum states of light [57,73]. The derived WPA theorem could be a useful method for accounting for nonlinear effects and related phenomena in various photon echo QM protocols in waveguides with three-level media, where the possibility of quantum storage on long-lived electron-nuclear spin quantum transitions poses new challenges.

ACKNOWLEDGMENTS

This research was supported by the Ministry of Science and Higher Education of the Russian Federation (Reg. No. NIOKTR 121020400113-1). S.P.K. and A.A.K. are supported by the Ministry of Science and Higher Education of the Russian Federation on the basis of the FSAEIH SUSU (NRU) (Grant Agreement No. 075-15-2022-1116).

APPENDIX A: HEISENBERG-LANGEVIN EQUATIONS OF LIGHT AND TWO-LEVEL ATOMS IN SINGLE-MODE WAVEGUIDE

For a more general description of the interaction between a light pulse and two-level atomic ensemble in a single waveguide, we will introduce the interaction of waveguide modes with their environment, where the total Hamiltonian \hat{H}_0 in Eq. (1) is supplemented by two members and takes the form $\hat{H} = \hat{H}_0 + \hat{H}_b + \hat{V}_{bf}$, where $\hat{H}_b = \hbar \sum_{n=1}^{N_w} \int d\omega_n \omega_n \hat{b}^\dagger(\omega_n) \hat{b}(\omega_n)$ is the Hamiltonian of the local spatial bath modes (N_w is its number) and $\hat{V}_{bf} = \hbar \sum_n f_n \hat{a}^\dagger(z_n) e^{-i\beta z_n} \hat{B}_n + \text{H.c.}$ [where $\hat{B}_n = \int d\omega_n \hat{b}(\omega_n)$, f_n is a coupling constant of field mode with bath modes at z_n , below we assume $f_n = f$ for simplicity] is interaction of bath modes with the light field modes; interaction with local reservoir modes leads to the irreversible attenuation of the light modes, in particular, when they are scattered on the inhomogeneities of waveguide walls.

Using \hat{H} , we derive a Heisenberg-Langevin equation for the field mode operator $\hat{a}_0(z, t)$ following the derivation of Eq. (10) and use the well-known input-output formalism [2,74] for calculating the relaxation terms and Langevin forces:

$$\begin{aligned} & \left(\frac{\partial}{\partial t} + \frac{\gamma_w}{2} + v_g \frac{\partial}{\partial z} \right) \hat{a}_0(z, t) \\ &= \frac{i}{2} \sum_{m=1}^M \sum_{j=1}^{N_m} \Omega_{0,m}(\mathbf{r}_\perp^j) \hat{\sigma}_{-,m}^j(t) \delta(z - z_j) + \sqrt{\gamma_w} \hat{b}_{in}(z, t), \end{aligned} \quad (\text{A1})$$

where Eq. (A1) differs from Eq. (10) by an appearance of the relaxation term $\frac{\gamma_w}{2} \hat{a}_0(z, t)$ and Langevin force $\hat{b}_{in}(z, t) = -i \sqrt{\frac{2\pi}{\gamma_w}} f^* \sum_n \hat{B}_n(t \rightarrow -\infty) e^{-i(\omega_n - \omega_0)(t - t_0)} \delta(z - z_n)$ (where $\langle \hat{b}_{in}(z, t) \rangle = 0$, $[\hat{b}_{in}(z, t) \hat{b}_{in}^\dagger(z', t')] = \delta(z - z')$

$\delta(t - t')$), coupling constant $\Omega_{0,m}(\mathbf{r}_\perp^j)$, and group velocity v_g are discussed after Eq. (1), $\gamma_w = 2\pi^2 |f|^2 \rho$ is a loss rate of waveguide modes related to the Langevin force ($\rho = N_w/L$, L = length of the waveguide).

The local operators $\frac{\gamma_w}{2} \hat{a}_0(z, t)$ and $\hat{b}_{in}(z, t)$ describe the light decay in the waveguide and Langevin forces in the continuous medium, where $\hat{b}_{in}(z, t)$ is determined by the input local fields $\hat{b}(\omega_n, t \rightarrow -\infty)$. Therefore, by introducing local noise operators $\hat{b}_{out}(z, t)$ at $t \rightarrow \infty$ similarly to the resonator input-output approach [74], we get the following local relation:

$$\hat{b}_{in}(z, t) - \hat{b}_{out}(z, t) = \sqrt{\gamma_w} \hat{a}_0(z, t). \quad (\text{A2})$$

The relation (A2) is useful for describing the absorption of a light pulse and can be applied to consider echo signals in waveguides where the absorbed signal is localized in the excited (bath) modes of the medium (waveguide) and can be recovered from them by controlled rephasing. Together with field (A1), we similarly derive Heisenberg-Langevin equations for the resonant atoms [2], limiting ourselves only to taking into account the influence of weak phase relaxation:

$$\begin{aligned} \frac{\partial \sigma_{-,m}^j}{\partial t} &= -(\gamma/2 + i\Delta_j) \sigma_{-,m}^j \\ &\quad - \frac{i}{2} \Omega_{0,m}(\mathbf{r}_\perp^j) \hat{a}_0(z_j, t) \sigma_{3,m}^j + \sqrt{\gamma} \hat{F}_{j,m}, \end{aligned} \quad (\text{A3})$$

$$\begin{aligned} \frac{\partial \sigma_{+,m}^j}{\partial t} &= -(\gamma/2 - i\Delta_j) \sigma_{+,m}^j \\ &\quad + \frac{i}{2} \Omega_{0,m}(\mathbf{r}_\perp^j) \hat{a}_0^\dagger(z_j, t) \sigma_{3,m}^j + \sqrt{\gamma} \hat{F}_{j,m}^\dagger, \end{aligned} \quad (\text{A4})$$

$$\frac{\partial \sigma_{3,m}^j}{\partial t} = -i\Omega_{0,m}(\mathbf{r}_\perp^j) [\hat{a}_0^\dagger(z_j, t) \sigma_{-,m}^j - \hat{a}_0(z_j, t) \sigma_{+,m}^j]. \quad (\text{A5})$$

Equations (A3)–(A5) of j th atom contain only pure dephasing decay constant γ with related Langevin forces $\sqrt{\gamma} \hat{F}_{j,m}(t)$ and $\sqrt{\gamma} \hat{F}_{j,m}^\dagger(t)$ [where $\langle \hat{F}_j(t) \hat{F}_{j'}^\dagger(t') \rangle = \delta_{j,j'} \delta(t - t')$] that are assumed to be identical for all the atoms, $\Delta_j(t) = \Delta_j + \delta\Delta_j(t)$, Δ_j and $\delta\Delta_j(t)$ are the static and fluctuating frequency offsets of j th atom, where Δ_j are inhomogeneous broadened by spectral distribution $G(\frac{\Delta}{\Delta_{in}})$, and Δ_{in} is a linewidth [1].

Introducing the density operators of photon number $\hat{I}_p(z, t) = \hat{a}_p^\dagger(z, t) \hat{a}_p(z, t)$ and atomic inversion $\hat{\sigma}_3(z, t) = \sum_{m=1}^M \sum_{j=1}^{N_m} \hat{\sigma}_{3,m}^j(t) \delta(z - z_j)$ and using Eqs. (A1) and (A5) we get the following waveguide equation for these operators, describing the behavior of the energy flow:

$$\partial_t (\hat{I}_p + \frac{1}{2} \hat{\sigma}_3) + v_g \partial_z \hat{I}_p = -\gamma_w \hat{I}_p + \sqrt{\gamma_w} \hat{M}_{p,b}, \quad (\text{A6})$$

where the two-particle operator $\hat{M}_{p,b} = \hat{a}_p^\dagger(z, t) \hat{b}_{in}(z, t) + \text{H.c.}$, the quantum mechanical average of which is zero due to the independent nature of the noise operator $\hat{b}_{in}(z, t)$ and $\langle \hat{b}_{in}(z, t) \rangle = 0$. Equation (A6) is valid for arbitrary constants of light-atom interaction, so it hides a specific dynamics under study. In the case of spatially localized 2π excitation (2π -echo sequence in Sec. III), the analytical solution of the field and atomic operators takes the form $\hat{I}_p(z, t) = \hat{I}_p(\xi)$, $\hat{\sigma}_3(z, t) = \hat{\sigma}_3(\xi)$, which satisfy the equation

$$\hat{\sigma}_3(\xi) = \hat{\sigma}_3(-\infty) + 2 \left(\frac{v_g}{\hat{v}_g} - 1 \right) [\hat{I}_p(\xi) - \hat{I}_p(-\infty)], \quad (\text{A7})$$

under the conditions of negligible relaxation, where $\hat{\sigma}_3(-\infty)$ and $\hat{I}_p(-\infty)$ are the initial atomic and field operators, $\xi = t - \frac{z}{\tilde{v}_g}$, \tilde{v}_g is a group velocity of the light-atoms (polariton) packet which is less than initial group velocity v_g of light without atomic medium and should be found as a result of solving a system of Eqs. (10)–(13) [i.e., Eqs. (A1)–(A5) not containing relaxation terms]. It is worth noting the exact analytical solution of the quantum Maxwell-Bloch Eqs. (10)–(13) with the identical constants of the light-atom interaction [75], demonstrating the possibility of quantum 2π solitons. However, Eqs. (A6) and (A7) also indicate the possibility of propagation of light pulses at a constant group velocity even in the presence of a spread of the constants of light-atom interaction.

Equations (A1)–(A5) should be solved for the stages of storage and retrieval of the fields in arbitrary quantum states. In the main part of work we focus on the consideration of the classical light fields, moving from the field operators $\hat{a}_m(z, t)$ to the c numbers $a_p(z, t) = e^{-i\phi} \langle \hat{a}_p(z, t) \rangle = e^{i\phi} \langle \hat{a}_p^\dagger(z, t) \rangle$, p ($s; 1; 2; e$) index indicating signal, controls, and echo pulses (see comments to Eq. (13) and omitting the Langevin forces [$\langle \hat{b}_{in}(z, t) \rangle = 0$]). At the same time, it should be noted that the semiclassical Maxwell-Bloch equations can be applied to describe the coherent interaction between light fields weakened to a single-photon level with atomic media [see also comments after Eq. (13)]. A number of basic properties of optical quantum memory protocols, such as the efficiency of signal pulse storage and the accuracy of its retrieval, can be also analyzed.

APPENDIX B: ROSE PROTOCOL IN OPTICALLY DENSE WAVEGUIDE

Here we assume that the signal and control fields have the same carrier frequency and do not have additional phase modulation. Using $w_m^{re}(\mathbf{r}_\perp, z)$ and $P_m^{re}(\mathbf{r}_\perp, z)$ in (44) together with phase relaxation function $\Gamma(\mathbf{r}, \tau, T_M, \Theta_{1,2})$ we can perform general analysis of nonlinear pattern in ROSE-pulse area behavior. In the simplest case of negligible spatial dependence of phase relaxation [i.e., $\Gamma(\mathbf{r}, \tau, T_2, \Theta_{1,2}) = \Gamma(\tau, T_2, \dots)$], we can perform integration and subsequent analytical calculation of (44) similar to (43) and to get the following equation for the envelope area of ROSE pulse:

$$\left(\frac{\partial}{\partial z} + \frac{\gamma_w}{2v_g} \right) \theta_e = \sum_{m=1}^M \frac{\varkappa_m}{\Omega_m} \left\{ \frac{\Gamma(\tau, T_M, \dots)}{4} I_{s,m}(\theta_s, \theta_1, \theta_2, \theta_e) - S_m(\theta_e; \theta_1; \theta_2) \right\}, \quad (\text{B1})$$

where a source of echo signal

$$\begin{aligned} I_{s,m}(\theta_s, \theta_1, \theta_2, \theta_e) &= \frac{1}{2} \Omega_m \theta_s(z) + S_m(\theta_s; \theta_e) + S_m(\theta_s; \theta_1; \theta_2) \\ &\quad - S_m(\theta_s; \theta_e; \theta_1) - S_m(\theta_s; \theta_e; \theta_2) + S_m(\theta_s; \theta_e; \theta_1; \theta_2), \end{aligned} \quad (\text{B2})$$

envelope areas $\theta_{s,1,2,e}(z)$ are all the functions of z , we also have taken into account that the signal pulse is weak

$$\Omega_m \theta_s(z) \ll \pi:$$

$$\begin{aligned} S_m(\theta_1; \theta_2; \theta_3) &= \frac{1}{4} \sum_{n=1}^2 \sum_{m=1}^2 \frac{\sin^2(\Omega_m[\theta_1 + (-1)^n \theta_2 + (-1)^m \theta_3]/2)}{\Omega_m[\theta_1 + (-1)^n \theta_2 + (-1)^m \theta_3]/2}, \\ S_m(\theta_1; \theta_2; \theta_3; \theta_4) &= \frac{1}{8} \sum_{n=1}^2 \sum_{m=1}^2 \sum_{p=1}^2 \\ &\quad \times \frac{\sin^2(\Omega_m[\theta_1 + (-1)^n \theta_2 + (-1)^m \theta_3 + (-1)^p \theta_4]/2)}{\Omega_m[\theta_1 + (-1)^n \theta_2 + (-1)^m \theta_3 + (-1)^p \theta_4]/2}. \end{aligned} \quad (\text{B3})$$

Equation (B1) is still a nonlinear equation on θ_e . In the case of atomic medium with limited optical density and weak input signal pulse, this equation reduces to the linear equation where $\Omega_m \theta_e(z) \ll \pi$. Neglecting the terms with $(\Omega_m \theta_e)^2 \ll \pi$ in (B1), we get

$$\left(\frac{\partial}{\partial z} + \frac{\gamma_w}{2v_g} \right) \theta_e = \sum_{m=1}^M \left\{ \frac{\varkappa_m}{4\Omega_m} \Gamma(\tau, T_2, \dots) I_{s,m}(\theta_s, \theta_{c1}, \theta_{c2}) - \frac{1}{2} \varkappa_m(\theta_{c1}; \theta_{c2}) \theta_e \right\}, \quad (\text{B4})$$

where $I_{s,m}(\theta_s, \theta_1, \theta_2) \equiv I_{s,m}(\theta_s, \theta_1, \theta_2, 0)$:

$$\begin{aligned} I_{s,m}(\theta_s, \theta_1, \theta_2) &= \Omega_m \theta_s - S_m(\theta_s; \theta_1) \\ &\quad - S_m(\theta_s; \theta_2) + 2S_m(\theta_s; \theta_1; \theta_2), \end{aligned} \quad (\text{B5})$$

and the absorption coefficient for echo signal due to the interaction with m th atomic group is

$$\begin{aligned} \varkappa_m(\theta_1; \theta_2) &= \varkappa_m \sum_{n=1}^2 \left\{ \frac{\sin[\Omega_m(\theta_1 + (-1)^n \theta_2)]}{\Omega_m[\theta_1 + (-1)^n \theta_2]} \right. \\ &\quad \left. - \frac{\sin^2[\Omega_m(\theta_1 + (-1)^n \theta_2)/2]}{2(\Omega_m(\theta_1 + (-1)^n \theta_2)/2)^2} \right\}. \end{aligned} \quad (\text{B6})$$

Equation (B4) is used in the main text.

APPENDIX C: EXCITATION OF ATOMS BY CONTROLLING CHIRPED PULSES

Here following the work [68], we consider the excitation of two-level atoms by two chirped control pulses. In the interaction picture, the equations for atomic amplitudes in the ground $C_2(t)$ and excited $C_1(t)$ states are

$$\begin{pmatrix} \dot{C}_1(t) \\ \dot{C}_2(t) \end{pmatrix} = \frac{i}{2} \begin{pmatrix} 0 & \Omega(t) \\ \Omega^*(t) & 0 \end{pmatrix} \begin{pmatrix} C_1(t) \\ C_2(t) \end{pmatrix}, \quad (\text{C1})$$

with initial state $C_2(t \rightarrow -\infty) = 1$, $C_1(t \rightarrow -\infty) = 0$, where

$$\begin{aligned} \Omega(t) &= \Omega_1(t - t_1) + \Omega_2(t - t_2) \\ &= [\dot{A}_1(t) e^{-iB_1(t)} + \dot{A}_2(t) e^{-iB_2(t)}] e^{-i\Delta(t-t_0)}, \end{aligned} \quad (\text{C2})$$

$$\dot{A}_p(t) = \frac{\chi_p}{\pi \tau_p} \frac{e^{-i\varphi_p}}{\cosh[(t - t_p)/\tau_p]}, \quad (\text{C3})$$

$$\dot{B}_p(t) = \frac{\beta_p}{\pi \tau_p} \tanh[(t - t_p)/\tau_p], \quad (\text{C4})$$

where the index $p = 1, 2$ corresponds to the first and second control pulse, and $A_p(t)$ is a Rabi frequency of the chirped pulses. We assume that the Rabi frequency is also a function of transverse coordinate \mathbf{r}_\perp : $\chi_p(\mathbf{r}_\perp) = \chi_{p,0}f(\mathbf{r}_\perp)$; φ_p is constant phase; $B_p(p)$ describes frequency modulation; Δ is an atomic frequency offset, τ_p is a temporal duration of p control pulse, χ_p and β_p are the amplitude and frequency chirp of p th control pulse, and $f(\mathbf{r}_\perp)$ is a spatial shape in the cross section of light beam. Below, we have taken into account a Gaussian membrane function of the Rabi frequency for each control field: $\chi_p(\mathbf{r}_\perp) = \chi_{p,0}f_g(\mathbf{r}_\perp)$.

By taking into account that the chirped pulses are not overlapped with each other ($\tau_{1,2} \ll t_1 - t_0, t_2 - t_1$), we can solve Eqs. (C1) one by one. For each pulse the solution of (C1) can be written in terms of hypergeometric functions where it is convenient writing $C_p(t)$ via the variable

$$z_1(t) = \frac{1}{2}\{1 + \tanh[(t - t_1)/\tau_1]\}, \quad (\text{C5})$$

i.e., $C_p(t) = \tilde{C}_p(z_1)$ and determining the phase of the first light pulse φ_1 by setting $B_1(t) = \int_{t_0}^t dt' \dot{B}_1(t')$. The atomic amplitudes after the action of first control pulse (starting at $t = t_0$) are described by

$$\tilde{C}_1(z_1) = A_1^{(12)} z_1^{1-c_1} \mathcal{F}_1^{(1)}(z_1), \quad (\text{C6})$$

$$\tilde{C}_2(z_1) = C_2(t_0) \mathcal{F}_1^{(2)*}(z_1), \quad (\text{C7})$$

where we introduced an abbreviated notation for the hypergeometric functions:

$$\mathcal{F}_p^{(1)}(z_p) = F(a_p + 1 - c_p, b_p + 1 - c_p, 2 - c_p, z_p), \quad (\text{C8})$$

$$\mathcal{F}_p^{(2)*}(z_p) = F^*(a_p, b_p, c_p, z_p) = F(a_p^*, b_p^*, c_p^*, z_p), \quad (\text{C9})$$

$$A_1^{(12)} = \frac{i\chi_1 e^{-i\varphi_1}}{2\pi(1 - c_1)} C_2(t_0) \exp\left\{i\left(\Delta - \frac{\beta_1}{\pi\tau_1}\right)(t_0 - t_1)\right\}. \quad (\text{C10})$$

The values a_p, b_p, c_p can be found in [68]:

$$a_p = \frac{1}{2\pi} [(\chi_p^2 - \beta_p^2)^{\frac{1}{2}} - i\beta_p], \quad (\text{C11})$$

$$b_p = \frac{1}{2\pi} [-(\chi_p^2 - \beta_p^2)^{\frac{1}{2}} - i\beta_p], \quad (\text{C12})$$

$$c_p = \frac{1}{2} \left[1 + i \frac{\pi \Delta \tau_p - \beta_p}{\pi} \right]. \quad (\text{C13})$$

Interaction with the first pulse ends for $t - t_1 \gg \tau_1$ when $z_1 \rightarrow 1$ and the amplitudes $\tilde{C}_{1,2}(z = 1)$ are set unchanged. The probability to find atom in the excited state after the action of the first pulse [$\text{for the initial state } |C_2(t_0)| \cong 1$ in (C7)] is

$$\mathcal{P}_{11}(t_1) \equiv P_{11}(t \gg t_1 + \tau_1) = |\tilde{C}_1(1)|^2 = \sin^2(\Theta_1/2), \quad (\text{C14})$$

where

$$\begin{aligned} \frac{\chi_p^2 |\mathcal{F}_p^{(1)}(1)|^2}{4\pi^2 |1 - c_p|^2} &= \sin^2(\Theta_p/2) \\ &= \frac{\sin^2(\Phi_p/2) Ch^2(\beta_p/2) + \cos^2(\Phi_p/2) Sh^2(\beta_p/2)}{Ch\left(\frac{\beta_p + \pi \Delta \tau_p}{2}\right) Ch\left(\frac{\beta_p - \pi \Delta \tau_p}{2}\right)}, \end{aligned} \quad (\text{C15})$$

where $\Phi_p = (\chi_p^2 - \beta_p^2)^{\frac{1}{2}}$ and (C14) and (C15) are also used to define the nutation angle of two-level atom $\Theta_{p=1} = \Theta_1(\Delta, \beta_1, \Phi_1)$ caused by the action of the first pulse. By using (C15), we can easily calculate $|\mathcal{F}_1^{(2)}(1)|^2$ and the probability of atom to stay on the ground level $P_2(t \gg t_1 + \tau_1) = |C_2(t \gg t_1)|^2 = |\tilde{C}_2(1)|^2 = |\mathcal{F}_1^{(2)}(1)|^2 = 1 - |\tilde{C}_2(1)|^2 = \cos^2(\Theta_1/2)$, so we get

$$\begin{aligned} C_2(t \gg t_1) &= \mathcal{F}_1^{(2)*}(1) \\ &= \cos(\Theta_1/2) \exp\{-i\zeta_1(\Delta, \chi_1, \beta_1, \tau_1)\}, \end{aligned} \quad (\text{C16})$$

where $\zeta_1(\Delta, \chi_1, \beta_1, \tau_1) = -i \ln\{\mathcal{F}_1^{(2)}(1)/\cos(\Theta_1/2)\}$.

Interaction with the second control pulse occurs at t_2 with sufficiently large time delay after the first control pulse $t_2 - t_1 \gg \tau_1$. Let us choose a moment of time in the middle between the control pulses $t_m = \frac{t_1+t_2}{2}$. Using (C1) for $t > t_m$ and moving to new amplitudes $C_{2,0}(t) = C_2(t) \exp\{-\frac{i}{2}\Delta(t_m - t_0)\}$, $C_{1,0}(t) = C_1(t) \exp\{\frac{i}{2}\Delta(t_m - t_0)\}$, we can describe the interaction with the second pulse similarly to the interaction with the first pulse. Here we get the following system of equations for atomic amplitudes $C_{1,0}(t)$ and $C_{2,0}(t)$ ($t > t_m$), which takes into account the phase change of the second pulse at the moment of the beginning of interaction with the atom:

$$\begin{pmatrix} \dot{C}_{1,0}(t) \\ \dot{C}_{2,0}(t) \end{pmatrix} = \frac{i}{2} \begin{pmatrix} 0 & \Omega_2(t - t_m) \\ \Omega_2^*(t - t_m) & 0 \end{pmatrix} \begin{pmatrix} C_{1,0}(t) \\ C_{2,0}(t) \end{pmatrix}, \quad (\text{C17})$$

with initial amplitudes

$$C_{2,0}(t_m) = \tilde{C}_2(1) \exp\left\{-\frac{i}{2}\Delta(t_m - t_0)\right\}, \quad (\text{C18})$$

$$C_{1,0}(t_m) = \tilde{C}_1(1) \exp\left\{\frac{i}{2}\Delta(t_m - t_0)\right\}, \quad (\text{C19})$$

where $\Omega_2(t - t_m)$ is given in Eqs. (C2)–(C4), and the constant phase of the second light pulse φ_2 .

Similarly to the interaction with the first pulse, we move to the new time variable scale $z_2 = \frac{1}{2}(1 + \tanh[(t - t_2)/\tau_2])$ and find solutions of $C_{p,0}(t > t_m) = \tilde{C}_{p,0}(z_2)$ for the initial conditions $\tilde{C}_{p,0}(0) = C_{p,0}(t_m)$:

$$\tilde{C}_{1,0}(z_2) = C_{1,0}(t_m) \mathcal{F}_2^{(2)}(z_2) + A_2^{(12)} z_2^{1-c_2} \mathcal{F}_2^{(1)}(z_2), \quad (\text{C20})$$

$$\tilde{C}_{2,0}(z_2) = C_{2,0}(t_m) F_2^{(2*)}(z_2) + A_2^{(21)} z_2^{1-c_2^*} F_2^{(1*)}(z_2), \quad (\text{C21})$$

where

$$A_2^{(12)} = \frac{i\chi_2 e^{-i\varphi_2}}{2\pi(1 - c_2)} C_{2,0}(t_m) \exp\left\{i\left(\Delta - \frac{\beta_2}{\pi\tau_2}\right)(t_m - t_2)\right\}, \quad (\text{C22})$$

$$A_2^{(21)} = \frac{i\chi_2 e^{i\varphi_2}}{2\pi(1 - c_2^*)} C_{1,0}(t_m) \exp\left\{-i\left(\Delta - \frac{\beta_2}{\pi\tau_2}\right)(t_m - t_2)\right\}. \quad (\text{C23})$$

The probability of the atomic excitation $\mathcal{P}_{11}(t_2) \equiv P_{11}[t \gg (t_2 + \tau_2)] = |\tilde{C}_{1,0}(z_2 = 1)|^2$ after the interaction with two control pulses will be

$$\begin{aligned} \mathcal{P}_{11}(t_2) &= |\tilde{C}_{1,0}(1)|^2 = |C_{1,0}(t_m) \mathcal{F}_2^{(2)}(1)|^2 \\ &+ |A_2^{(12)} \mathcal{F}_2^{(1)}(1)|^2 + [\delta\mathcal{P}_{\text{coh}}(t_2) + \text{c.c.}], \end{aligned} \quad (\text{C24})$$

where we have

$$|C_{1,0}(t_m)\mathcal{F}_2^{(2)}(1)|^2 = \sin^2(\Theta_1/2)\cos^2(\Theta_2/2), \quad (\text{C25})$$

$$|A_2^{(12)}\mathcal{F}_2^{(1)}(1)|^2 = \sin^2(\Theta_2/2)\cos^2(\Theta_1/2), \quad (\text{C26})$$

and interference term

$$\begin{aligned} \delta\mathcal{P}_{\text{coh}}(t_2) &= C_{1,0}(t_m)A_2^{(12)*}\mathcal{F}_2^{(2)}(1) \\ &= \exp\{i[\delta\varphi + \tilde{\varphi}_{2,1} + \Delta(t_2 - t_1)]\} \\ &\quad \times \frac{\chi_1\chi_2\mathcal{F}_1^{(1)}(1)\mathcal{F}_2^{(1)*}(1)}{4\pi^2(1-c_1)(1-c_2^*)}\mathcal{F}_1^{(2)}(1)\mathcal{F}_2^{(2)}(1), \quad (\text{C27}) \end{aligned}$$

where $\delta\varphi$ is a random phase that is acquired by an atom during the time interval $t_2 - t_1$ of free evolution due to the interaction with bath fields, $\tilde{\varphi}_{2,1} = \tilde{\varphi}_2 - \tilde{\varphi}_1$, $\tilde{\varphi}_p$, and con-

stant phases of p th control pulses are defined by setting $B_{1,2}(t) = \int_{t_0}^t dt' \tilde{B}_2(t')$ as follows: $\tilde{\varphi}_1 = \varphi_1 + \frac{\beta_1}{\pi\tau_1}(t_0 - t_1)$, $\tilde{\varphi}_2 = \varphi_2 + \frac{\beta_2}{\pi\tau_2}(t_m - t_2)$. In (C27) we also used $C_{1,0}(t_m) = \tilde{C}_1(1)\exp\{\frac{i}{4}\Delta(t_m - t_0)\}$, $\tilde{C}_1(1) = A_1^{(12)}\mathcal{F}_1^{(1)}(1)$, and $C_{2,0}(t_m) = \tilde{C}_2(1)\exp\{-\frac{i}{4}\Delta(t_m - t_0)\}$, $\tilde{C}_2(1) = \mathcal{F}_1^{(2)*}(1)$.

In the particular case of identical two control pulses ($\chi_1 = \chi_2$, $\beta_1 = \beta_2$, $\tau_1 = \tau_2$, and $\Theta_1 = \Theta_2$, respectively), we get

$$\begin{aligned} \mathcal{P}_{11}(t_2; \Theta_2 = \Theta_1) \\ = \frac{1}{2}\sin^2\Theta_1\{1 + \cos[\delta\varphi + 2\zeta_1 + \Delta(t_2 - t_1)]\}, \quad (\text{C28}) \end{aligned}$$

where ζ_1 is given in Eq. (C16) and the durations of the control pulses are defined by $\tau_{1,2} = \delta t_{1,2}$ in the main text.

-
- [1] L. Allen and J. Eberly, *Optical Resonance and Two-level Atoms*, Dover Books on Physics and Chemistry (Dover, New York, 1975), p. 256.
- [2] M. O. Scully and M. S. Zubairy, *Quantum Optics* (Cambridge University Press, Cambridge, 1997).
- [3] R. W. Boyd, *Nonlinear Optics*, 2nd ed. (Academic, New York, 2003).
- [4] N. Sangouard, C. Simon, H. de Riedmatten, and N. Gisin, Quantum repeaters based on atomic ensembles and linear optics, *Rev. Mod. Phys.* **83**, 33 (2011).
- [5] S. L. McCall and E. L. Hahn, Self-induced transparency, *Phys. Rev.* **183**, 457 (1969).
- [6] R. Gutiérrez-Cuevas and J. H. Eberly, Vector-soliton storage and three-pulse-area theorem, *Phys. Rev. A* **94**, 013820 (2016).
- [7] C. Greiner, T. Wang, T. Loftus, and T. W. Mossberg, Instability and Pulse Area Quantization in Accelerated Superradiant Atom-Cavity Systems, *Phys. Rev. Lett.* **87**, 253602 (2001).
- [8] E. L. Hahn, N. S. Shiren, and S. L. McCall, Application of the area theorem to phonon echoes, *Phys. Lett. A* **37**, 265 (1971).
- [9] S. A. Moiseev, M. Sabooni, and R. V. Urmancheev, Photon echoes in optically dense media, *Phys. Rev. Res.* **2**, 012026(R) (2020).
- [10] S. A. Moiseev and R. V. Urmancheev, Photon/spin echo in a fabry-perot cavity, *Opt. Lett.* **47**, 3812 (2022).
- [11] J.-H. Kim, S. Aghaeimeibodi, J. Carolan, D. Englund, and E. Waks, Hybrid integration methods for on-chip quantum photonics, *Optica* **7**, 291 (2020).
- [12] Y. Hibino, Silica-based planar lightwave circuits and their applications, *MRS Bull.* **28**, 365 (2003).
- [13] A. Rodenas and A. K. Kar, High-contrast step-index waveguides in borate nonlinear laser crystals by 3D laser writing, *Opt. Express* **19**, 17820 (2011).
- [14] A. G. Okhrimchuk, A. V. Shestakov, I. Khrushchev, and J. Mitchell, Depressed cladding, buried waveguide laser formed in a YAG:Nd³⁺ crystal by femtosecond laser writing, *Opt. Lett.* **30**, 2248 (2005).
- [15] N. Sinclair, E. Saglamyurek, M. George, R. Ricken, C. L. Mela, W. Sohler, and W. Tittel, Spectroscopic investigations of a Ti:TM:LiNbO₃ waveguide for photon-echo quantum memory, *J. Lumin.* **130**, 1586 (2010).
- [16] E. Saglamyurek, N. Sinclair, J. Jin, J. A. Slater, D. Oblak, F. Bussi eres, M. George, R. Ricken, W. Sohler, and W. Tittel, Broadband waveguide quantum memory for entangled photons, *Nature (London)* **469**, 512 (2011).
- [17] S. Marzban, J. G. Bartholomew, S. Madden, K. Vu, and M. J. Sellars, Observation of Photon Echoes From Evanescently Coupled Rare-Earth Ions in a Planar Waveguide, *Phys. Rev. Lett.* **115**, 013601 (2015).
- [18] G. Corrielli, A. Seri, M. Mazzer, R. Osellame, and H. de Riedmatten, Integrated Optical Memory Based on Laser-Written Waveguides, *Phys. Rev. Appl.* **5**, 054013 (2016).
- [19] C. Liu, T.-X. Zhu, M.-X. Su, Y.-Z. Ma, Z.-Q. Zhou, C.-F. Li, and G.-C. Guo, On-Demand Quantum Storage of Photonic Qubits in an On-Chip Waveguide, *Phys. Rev. Lett.* **125**, 260504 (2020).
- [20] S. Wang, L. Yang, M. Shen, W. Fu, Y. Xu, R. L. Cone, C. W. Thiel, and H. X. Tang, Er : LiNbO₃ with High Optical Coherence Enabling Optical Thickness Control, *Phys. Rev. Appl.* **18**, 014069 (2022).
- [21] A. I. Lvovsky, B. C. Sanders, and W. Tittel, Optical quantum memory, *Nat. Photonics* **3**, 706 (2009).
- [22] K. Hammerer, A. S. Sørensen, and E. S. Polzik, Quantum interface between light and atomic ensembles, *Rev. Mod. Phys.* **82**, 1041 (2010).
- [23] W. Tittel, M. Afzelius, T. Chaneli ere, R. Cone, S. Kr oll, S. Moiseev, and M. Sellars, Photon-echo quantum memory in solid state systems, *Laser Photonics Rev.* **4**, 244 (2010).
- [24] F. Bussi eres, N. Sangouard, M. Afzelius, H. de Riedmatten, C. Simon, and W. Tittel, Prospective applications of optical quantum memories, *J. Mod. Opt.* **60**, 1519 (2013).
- [25] K. Heshami, D. G. England, P. C. Humphreys, P. J. Bustard, V. M. Acosta, J. Nunn, and B. J. Sussman, Quantum memories: emerging applications and recent advances, *J. Mod. Opt.* **63**, 2005 (2016).
- [26] T. Chaneli ere, G. H etet, and N. Sangouard, Quantum optical memory protocols in atomic ensembles, in *Advances In Atomic, Molecular, and Optical Physics*, edited by E. Arimondo, L. F. DiMauro, and S. F. Yelin (Academic, New York, 2018), Vol. 67, Chap. 2, pp. 77–150.
- [27] S. Wehner, D. Elkouss, and R. Hanson, Quantum internet: A vision for the road ahead, *Science* **362**, eaam9288 (2018).

- [28] J. Wang, F. Sciarrino, A. Laing, and M. G. Thompson, Integrated photonic quantum technologies, *Nat. Photonics* **14**, 273 (2020).
- [29] F. Kaneda, F. Xu, J. Chapman, and P. G. Kwiat, Quantum-memory-assisted multi-photon generation for efficient quantum information processing, *Optica* **4**, 1034 (2017).
- [30] M. Sabooni, Q. Li, S. Kröll, and L. Rippe, Efficient Quantum Memory using a Weakly Absorbing Sample, *Phys. Rev. Lett.* **110**, 133604 (2013).
- [31] M. P. Hedges, J. J. Longdell, Y. Li, and M. J. Sellars, Efficient quantum memory for light, *Nature (London)* **465**, 1052 (2010).
- [32] D. Schraft, M. Hain, N. Lorenz, and T. Halfmann, Stopped Light at High Storage Efficiency in a $\text{Pr}^{3+} : \text{Y}_2\text{SiO}_5$ Crystal, *Phys. Rev. Lett.* **116**, 073602 (2016).
- [33] C. W. Thiel, Y. Sun, R. M. Macfarlane, T. Böttger, and R. L. Cone, Rare-earth-doped LiNbO_3 and KTiOPO_4 (KTP) for waveguide quantum memories, *J. Phys. B: At., Mol. Opt. Phys.* **45**, 124013 (2012).
- [34] E. Saglamyurek, J. Jin, V. B. Verma, M. D. Shaw, F. Marsili, S. W. Nam, D. Oblak, and W. Tittel, Quantum storage of entangled telecom-wavelength photons in an erbium-doped optical fibre, *Nat. Photonics* **9**, 83 (2015).
- [35] C. Liu, Z.-Q. Zhou, T.-X. Zhu, L. Zheng, M. Jin, X. Liu, P.-Y. Li, J.-Y. Huang, Y. Ma, T. Tu, T.-S. Yang, C.-F. Li, and G.-C. Guo, Reliable coherent optical memory based on a laser-written waveguide, *Optica* **7**, 192 (2020).
- [36] A. Seri, G. Corrielli, D. Lago-Rivera, A. Lenhard, H. de Riedmatten, R. Osellame, and M. Mazzerà, Laser-written integrated platform for quantum storage of heralded single photons, *Optica* **5**, 934 (2018).
- [37] M. F. Askarani, M. G. Puigibert, T. Lutz, V. B. Verma, M. D. Shaw, S. W. Nam, N. Sinclair, D. Oblak, and W. Tittel, Storage and Reemission of Heralded Telecommunication-Wavelength Photons using a Crystal Waveguide, *Phys. Rev. Appl.* **11**, 054056 (2019).
- [38] A. Seri, D. Lago-Rivera, A. Lenhard, G. Corrielli, R. Osellame, M. Mazzerà, and H. de Riedmatten, Quantum Storage of Frequency-Multiplexed Heralded Single Photons, *Phys. Rev. Lett.* **123**, 080502 (2019).
- [39] S. A. Moiseev and S. Kröll, Complete Reconstruction of the Quantum State of a Single-Photon Wave Packet Absorbed by a Doppler-Broadened Transition, *Phys. Rev. Lett.* **87**, 173601 (2001).
- [40] S. A. Moiseev, V. F. Tarasov, and B. S. Ham, Quantum memory photon echo-like techniques in solids, *J. Opt. B: Quantum Semiclassical Opt.* **5**, S497 (2003).
- [41] B. Kraus, W. Tittel, N. Gisin, M. Nilsson, S. Kröll, and J. I. Cirac, Quantum memory for nonstationary light fields based on controlled reversible inhomogeneous broadening, *Phys. Rev. A* **73**, 020302(R) (2006).
- [42] M. Afzelius, C. Simon, H. de Riedmatten, and N. Gisin, Multimode quantum memory based on atomic frequency combs, *Phys. Rev. A* **79**, 052329 (2009).
- [43] V. Damon, M. Bonarota, A. Louchet-Chauvet, T. Chanelière, and J.-L. L. Gouët, Revival of silenced echo and quantum memory for light, *New J. Phys.* **13**, 093031 (2011).
- [44] M. M. Minnegaliev, K. I. Gerasimov, R. V. Urmancheev, A. M. Zheltikov, and S. A. Moiseev, Linear stark effect in $\text{Y}_3\text{Al}_5\text{O}_{12}:\text{Tm}^{3+}$ crystal and its application in the addressable quantum memory protocol, *Phys. Rev. B* **103**, 174110 (2021).
- [45] N. Skryabin, A. Kalinkin, I. Dyakonov, and S. Kulik, Femtosecond laser written depressed-cladding waveguide 2×2 , 1×2 and 3×3 directional couplers in $\text{Tm}_3 + : \text{YAG}$ crystal, *Micromachines* **11**, 1 (2020).
- [46] S. A. Moiseev, Some general nonlinear properties of photon-echo radiation in optically dense media, *Optika i Spektroskopiya* **62**, 302 (1987) [*Opt. Spectrosc.* **62**, 180 (1987)].
- [47] R. Urmancheev, K. Gerasimov, M. Minnegaliev, T. Chanelière, A. Louchet-Chauvet, and S. Moiseev, Two-pulse photon echo area theorem in an optically dense medium, *Opt. Express* **27**, 28983 (2019).
- [48] S. A. Moiseev, Quantum memory for intense light fields in the photon echo technique, *Izv. Ross. Akad. Nauk, Ser. Fiz.* **68**, 1260 (2004) [*Bull. Russ. Acad. Sci. Phys.* **68**, 1408 (2004)].
- [49] P. Goldner, A. Ferrier, and O. Guillot-Noel, *Rare Earth-doped Crystals for Quantum Information Processing* (Elsevier, Amsterdam, 2015), pp. 1–78.
- [50] J.-T. Shen and S. Fan, Theory of single-photon transport in a single-mode waveguide. I. coupling to a cavity containing a two-level atom, *Phys. Rev. A* **79**, 023837 (2009).
- [51] S. A. Moiseev and W. Tittel, Temporal compression of quantum-information-carrying photons using a photon-echo quantum memory approach, *Phys. Rev. A* **82**, 012309 (2010).
- [52] D. Roy, C. M. Wilson, and O. Firstenberg, Colloquium: Strongly interacting photons in one-dimensional continuum, *Rev. Mod. Phys.* **89**, 021001 (2017).
- [53] H. Kogelnik, *Theory of Optical Waveguides, in Guided-Wave Optoelectronics* (Springer, Berlin, 1988).
- [54] B. Huttner and S. M. Barnett, Quantization of the electromagnetic field in dielectrics, *Phys. Rev. A* **46**, 4306 (1992).
- [55] K. Okamoto, *Fundamentals of Optical Waveguides* (Elsevier, Amsterdam, 2021).
- [56] E. S. Moiseev and S. A. Moiseev, Scalable time reversal of raman echo quantum memory and quantum waveform conversion of light pulse, *New J. Phys.* **15**, 105005 (2013).
- [57] E. S. Moiseev, A. Tashchilina, S. A. Moiseev, and A. I. Lvovsky, Darkness of two-mode squeezed light in lambda-type atomic system, *New J. Phys.* **22**, 013014 (2020).
- [58] F. Haake, H. King, G. Schröder, J. Haus, and R. Glauber, Fluctuations in superfluorescence, *Phys. Rev. A* **20**, 2047 (1979).
- [59] G. L. Lamb, Analytical descriptions of ultrashort optical pulse propagation in a resonant medium, *Rev. Mod. Phys.* **43**, 99 (1971).
- [60] W. B. Mims, Phase memory in electron spin echoes, lattice relaxation effects in $\text{CaWO}_4 : \text{Er, Ce, Mn}$, *Phys. Rev.* **168**, 370 (1968).
- [61] R. L. Cone and G. K. Liu, Power-dependent photon echo decay due to instantaneous diffusion' in $\text{Tb}_3 + : \text{LiYF}_4$, *Bull. Am. Phys. Soc.* **33**, 676 (1988).
- [62] C. W. Thiel, R. M. Macfarlane, Y. Sun, T. Böttger, N. Sinclair, W. Tittel, and R. L. Cone, Measuring and analyzing excitation-induced decoherence in rare-earth-doped optical materials, *Laser Phys.* **24**, 106002 (2014).
- [63] M. M. Minnegaliev, K. I. Gerasimov, T. N. Sabirov, R. V. Urmancheev, and S. A. Moiseev, Implementation of an

- optical quantum memory protocol in the $^{167}\text{Er}^{3+} : \text{Y}_2\text{SiO}_5$ crystal, *JETP Lett.* **115**, 720 (2022).
- [64] T. Chanelière, M. Bonarota, V. Damon, R. Lauro, J. Ruggiero, I. Lorgere, and J.-L. L. Gouët, Light storage protocols in Tm:YAG, *J. Lumin.* **130**, 1572 (2010), special Issue based on the Proceedings of the Tenth International Meeting on Hole Burning, Single Molecule, and Related Spectroscopies: Science and Applications (HBSM 2009), issue dedicated to Ivan Lorgere and Oliver Guillot-Noel.
- [65] See code and simulation details at <https://github.com/Eugene91/YAG-waveguide>.
- [66] S. A. Moiseev and M. I. Noskov, The possibilities of the quantum memory realization for short pulses of light in the photon echo technique, *Laser Phys. Lett.* **1**, 303 (2004).
- [67] N. Sangouard, C. Simon, M. Afzelius, and N. Gisin, Analysis of a quantum memory for photons based on controlled reversible inhomogeneous broadening, *Phys. Rev. A* **75**, 032327 (2007).
- [68] F. T. Hioe, Solution of bloch equations involving amplitude and frequency modulations, *Phys. Rev. A* **30**, 2100 (1984).
- [69] M. M. Minnegaliev, I. V. Dyakonov, K. I. Gerasimov, A. A. Kalinkin, S. P. Kulik, S. A. Moiseev, M. Y. Saygin, and R. V. Urmancheev, Observation and investigation of narrow optical transitions of $^{167}\text{Er}^{3+}$ ions in femtosecond laser printed waveguides in $^7\text{LiYF}_4$ crystal, *Laser Phys. Lett.* **15**, 045207 (2018).
- [70] E. S. Moiseev, A. Tashchilina, S. A. Moiseev, and B. C. Sanders, Broadband quantum memory in a cavity via zero spectral dispersion, *New J. Phys.* **23**, 063071 (2021).
- [71] J. Dajczgewand, R. Ahlefeldt, T. Böttger, A. Louchet-Chauvet, J.-L. Le Gouët, and T. Chanelière, Optical memory bandwidth and multiplexing capacity in the erbium telecommunication window, *New J. Phys.* **17**, 023031 (2015).
- [72] G. T. Campbell, O. Pinel, M. Hosseini, T. C. Ralph, B. C. Buchler, and P. K. Lam, Configurable Unitary Transformations and Linear Logic Gates using Quantum Memories, *Phys. Rev. Lett.* **113**, 063601 (2014).
- [73] S. E. Beavan, M. P. Hedges, and M. J. Sellars, Demonstration of Photon-Echo Rephasing of Spontaneous Emission, *Phys. Rev. Lett.* **109**, 093603 (2012).
- [74] D. Walls and G. Milburn, *Quantum Optics* (Springer, Berlin, 2008).
- [75] V. I. Rupasov, Contribution to the dicke superradiance theory. exact solution of the quasi-one-dimensional quantum model, *Zh. Eksp. Teor. Fiz.* **83**, 1711 (1982) [*Sov. Phys.–JETP* **56**, 989 (1982)].